Two-Way Satellite-HAP-Terrestrial Networks with Non-Orthogonal Multiple Access

Kefeng Guo, Haifeng Shuai, Xingwang Li, *Senior Member, IEEE*, Liang Yang, *Member, IEEE*, Theodoros A. Tsiftsis, *Senior Member, IEEE*, Arumugam Nallanathan, *Fellow, IEEE* and Min Wu

***Abstract*—Satellite-high altitude platform (HAP)-terrestrial networks have been considered as an indispensable infrastructure of next-generation networks because they can offer massive access service with high throughput and broad coverage connections. Meanwhile, non-orthogonal multiple access (NOMA) and two-way relaying techniques are considered as potential technologies to enhance the spectrum efficiency and connectivity. Thus, in this paper, the performance of two-way satellite-HAP-terrestrial networks with NOMA, which are subject to imperfect channel state information and successive interference cancellation, is investigated. Closed-form and asymptotic expressions for the outage probability, and ergodic capacity are derived to verify the impact of the system and channel parameters on the considered network. Simulation results indicate that the optimization power allocation factor is independent of the channel fading.**

***Index Terms*—Imperfect channel state information (CSI), imperfect successive interference cancellation (SIC), non-orthogonal multiple access (NOMA), satellite-high altitude platform-terrestrial networks (ISHAP-TNs), two-way relaying.**

I. Introduction

HIGH-quality, high-throughput, ultra-reliability, low latency, and massive connectivity are the major requirements for next-generation wireless communication networks [1]–[3]. On this foundation, the structure for integrated satellite-aerial-terrestrial networks have gained considerable interest [4]–[6]. Among satellite-aerial-terrestrial networks, the integrated satellite-high altitude platform (HAP)-terrestrial networks (IS-HAP-TNs) combine the following advantages the wide coverage and invulnerability of satellite networks, the maturity and high-quality transmission of terrestrial networks, and the flexibility of aerial networks [7]–[9]. Owing to the fact that HAP always works as a relay in the stratosphere, so that when compared with the satellite transmission links, the HAP-terrestrial link has its own advantages, such as lower latency, more flexibility and wider coverage [10], [11].

As mentioned before, due to the rapidly development of internet-of-things (IoT) and internet-of-vehicles (IoV) technologies, a tremendous number of wireless devices need access to wireless networks [12], [13]. Massive access and high spectrum utilization efficiency have been as basic requirements of next-generation networks [14]–[16]. Consequently, non-orthogonal multiple access (NOMA) can distribute the same time/frequency/code resource block to different users that rely on the power domain, which is considered as a promising candidate of the next-generation multiple access [17]–[19]. Unlike the traditional orthogonal multiple access (OMA) scheme, NOMA can effectively increase the number of access users and enhance the system spectrum efficiency. Another technique to improve the spectrum efficiency is the two-way relay technology, which improve the spectrum efficiency by reducing the time slots [20]–[22]. Therefore, it is very necessary for the next-generation networks to both utilize the NOMA and two-way technology into the satellite-HAP-terrestrial networks [23]–[25].

A. Technical Literature Review and Motivation

Recently, IS-HAP-TNs have attracted great attention of the academic and industrial circles [26]–[28]. To evaluate the performance of IS-HAP-TNs, the outage probability (OP) and ergodic capacity (EC) are useful performance indicators [29], [30]. The authors in [31] investigated the performance of a non-stationary satellite communication system, where closed-form and asymptotic expressions for the instantaneous OP, EC and throughput were deduced. In addition, unmanned aerial vehicles (UAVs) have been used on a large scale as relay nodes. In [32], the authors established a three-dimensional integrated satellite-UAV-terrestrial system with UAV, and the EC was derived. To verify the timeliness and reliability of the satellite-aerial-terrestrial network, the authors of [33] discussed the delay and outage for the satellite-aerial-terrestrial network. In [34], the authors formulated a non-convex optimization problem to maximize the sum rate of an IS-HAP-TN. In [36], the authors investigated the secrecy problem of the IS-HAP-TN with the assistance of reconfigurable intelligent surface.

On the other hand, NOMA can improve the connectivity and spectrum efficiency, so it is widely employed in IS-HAP-TNs [35]. In [37], the outage behavior of NOMA-based

This work was supported by the National Science Foundation of China under Grant 62001517. (The corresponding author: Haifeng Shuai, email: shuaihf99@163.com; The co-corresponding author is Xingwang Li, email: lixingwangbupt@ gmail.com).

K. Guo and M. Wu are with the School of Space Information, Space Engineering University, Beijing, 101416, China (e-mail: guokefeng.cool@163.com; 1800022837@pku.edu.cn).

H. Shuai is with the Beijing Special Engineering Design and Research Institute, Beijing, 100028, China (e-mail: shuaihf99@163.com)

X. Li is with the School of Physics and Electronic Information Engineering, Henan Polytechnic University, Jiaozuo, 454000, China (e-mail: lixingwangbupt@gmail.com).

L. Yang is with the College of Information Science and Engineering, Hunan University, Changsha, 410082, China (e-mail: liangy@hnu.edu.cn).

T. A. Tsiftsis is with the Department of Informatics and Telecommunications, University of Thessaly, Lamia 35100, Greece (email: tsiftsis@uth.gr).

A. Nallanathan is with the School of Electronic Engineering and Computer Science, Queen Mary University of London, London E1 4NS, U.K. (e-mail: a.nallanathan@qmul.ac.uk).

hybrid satellite-UAV-terrestrial networks was analyzed, and the sum rate of the considered system was maximized through UAV location optimization. The authors of [38] studied a system model applying intelligent reflecting surface (IRS) and NOMA techniques to wireless systems. In [39], the authors investigated NOMA schemes in UAV-aided ground-air-ground communication networks, and evaluated the network outage performance and throughput, with simulation results showing proof that NOMA scheme outperforms OMA scheme. The authors of [40] analyzed a cooperative NOMA-based cognitive radio network, besides, the authors proved that the cooperative scheme was proven to achieve the maximum diversity order. The cooperative NOMA scheme was investigated in [41] to alleviate shadowing effects at poor channel users in an integrated satellite terrestrial relay network. In [42], the authors studied the NOMA-based cognitive mobile communication system with imperfect channel estimation. In [43], the outage performance of NOMA-based FSO-RF systems with a dual energy harvesting mode was investigated. In [44], the authors investigated a buffer-aided cooperative relaying system with multiple relays and a direct link from the source to the destination, providing a general scenario different from other existing state-of-the-art techniques. In [45], a wireless power transfer assisted uplink NOMA (WPT-NOMA) network in IoT was considered, where the battery-less IoT devices harvest the energy from the dedicated access point, based on linear and non-linear energy harvesting (EH) models.

Nevertheless, most of the above published works rely on the one-way relay protocol. To improve the communication efficiency, users can simultaneously communicate with one another via a two-way relay [46]. In [47], the authors proved that the performance of the two-way relay NOMA system was better than that of the two-way relay OMA system. Moreover, in [48], the authors investigated the OP, diversity order, and throughput to measure a full duplex two-way relay NOMA system. In [49], the authors adopted an IRS in multi-user two-way relay networks, and designed a user scheduling scheme to improve the secrecy rate.

For wireless communication networks, due to the fast scattering and propagation errors, perfect channel state information (CSI) is difficult to acquire, especially in satellite and aerial channels [50]. The authors of [51] analyzed the performance of the OP and intercept probability caused by imperfect CSI in a NOMA-based ambient backscatter system. The energy efficiency of the satellite terrestrial network under imperfect CSI was analyzed in [52]. A NOMA-based uplink satellite network was investigated in [53], and obtained the EC under imperfect CSI and antenna-pointing error. Therefore, the impacts of imperfect CSI on the performance of the IS-HAP-TNs [54] should be investigated.

When signals are being received, successive interference cancellation (SIC) is adopted in NOMA systems [55], [56]. However, due to complexity scaling, propagation and synchronization errors, the SIC technology is difficult to be implemented perfectly [57], [58]. The authors of [59] investigated the OP performance of NOMA-based satellite network under imperfect SIC, while an independent factor was utilized to verify the effect of imperfect SIC. The same assumption of imperfect SIC was also adopted in [60], where the authors analyzed cooperative NOMA networks with multiple full-duplex decode-and-forward relays and proposed an adaptive power allocation scheme under imperfect SIC. Based on the state-of-the-art, it is clear that both NOMA and two-way relay techniques can enhance the traverse rate performance of IS-HAP-TNs. This is precisely the motivation for the study in this paper.

B. Our Contribution

In this paper, by implementing NOMA technology, two-way relaying transmission under practical limitations, i.e., imperfect CSI and SIC, the major contributions are as follows:

- Firstly, we establish a general model for the two-way satellite-HAP-terrestrial network with NOMA. The HAP works as a two-way relay to guarantee the communication between the satellite and the terrestrial user by utilizing the half-duplex decode-and-forward (DF) protocol.
- Secondly, by considering the limitations in the transmission process, i.e., imperfect CSI and SIC into IS-HAP-TNs, we obtain signal-to-interference-plus-noise ratio (SINR) of the signal decoded at each node under imperfect limitations. Based on these limitations, closed-form expressions for the OP and EC are obtained.
- Thirdly, to gain further insights, we get the asymptotic expression for OP in high signal-to-noise ratio (SNR) regime. where the effects of channel and system parameters on the OP are highlighted.
- Finally, theoretical results are verified by Monte Carlo simulations. Some interesting findings are obtained from the simulation results.

C. Organization

The main structure of this paper is as follows. Section II introduces the system model, the problem formulation based on signal transmission, and the proposed channel models. Then, theoretical derivations for the OP and EC are obtained in Section III. In Section IV, the theoretical derivations of the considered network are verified by Monte Carlo simulations. Finally, some concluding remarks are given in Section V.

II. System Model and Problem Formulation

Fig. 1 illustrates a two-way IS-HAP-TNs with NOMA, which consists of a satellite, multiple terrestrial users, and multiple two-way HAPs[1]. The terrestrial users are equipped with one antenna[2]. The HAPs act as two-way half-duplex DF relays[3]. Firstly, by the layered coding technology, the

[1]In this paper, we focus on one satellite beam and one HAP with the same coverage. The satellite and terrestrial users exchange signals with each other through either direct links or HAP-assisted links.

[2]It is mentioned that, in this paper, the terrestrial nodes are equipped with only one antenna, while the results are also suitable to the case that transmission nodes are equipped with multiple antennas and beamforming (BF) is utilized at each multiple antenna node.

[3]Although only one HAP is employed for the two terrestrial users, the derived results can be considered as a special case of multiple HAPs scenario.

satellite (S) and terrestrial user (U)[4] transmit a superposed signal to each other via the HAP. Next, the two-way HAP utilizes the superposition coding technology to obtain the superimposed signal from the decoded source signal. Finally, it simultaneously transmits the signal to the satellite and user[5]. In addition, the HAP employs a receive antenna and a transmit antenna, respectively, to communicate with the two signal sources [27].

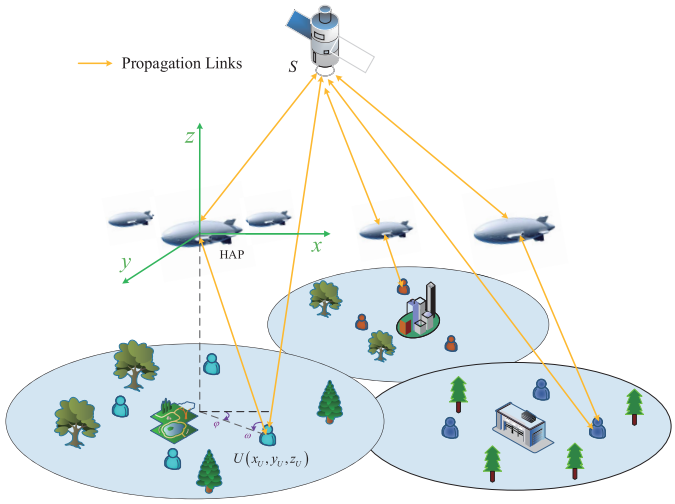

Fig. 1. Illustration of a two-way satellite-HAP-terrestrial network with NOMA.

A. Signal Model

The proposed system contains two transmission phases. In the first phase, the satellite and terrestrial user transmit their own superimposed signals through the layered coding technology[6]. The superposition signal of S can be expressed as $y_S = \sqrt{a_1}x_s + \sqrt{a_2}x_{s'}$, where the satellite divides its own signal into a basic layer signal x_s and an additional layer signal $x_{s'}$, which satisfies $E\left[|x_s|^2\right] = E\left[|x_{s'}|^2\right] = 1$, where $E[\cdot]$ denotes the expectation operation. a_1 and a_2 are the power allocation coefficients of S, which satisfy $a_1 + a_2 = 1$. To guarantee the quality of the signal, more power is allocated to x_s, i.e., $a_1 > a_2$ [24]. Similarly, the terrestrial user divides its own signal into a basic layer signal x_u and an additional layer signal $x_{u'}$, which can be expressed as $y_U = \sqrt{b_1}x_u + \sqrt{b_2}x_{u'}$ with $E\left[|x_u|^2\right] = E\left[|x_{u'}|^2\right] = 1$. b_1 and b_2 are the power allocation coefficients of U, which satisfy $b_1 + b_2 = 1$ and $b_1 > b_2$. Therefore, the signal received by the terrestrial user from the satellite can be expressed as

$$z_{U_1} = \sqrt{P_S}h_{SU}\left(\sqrt{a_1}x_s + \sqrt{a_2}x_{s'}\right) + n_U, \tag{1}$$

where P_S is the power of the satellite transmitted signal. $P_S = \mu P_E$, P_E is the entire power of the satellite transmission, and $\mu \in (0,1)$ is the power coefficient allocated for the signal transmission, whereas the remainder of the entire power is allocated to the pilot symbol to estimate the CSI. h_{SU} is the complex propagation coefficient between the satellite and the user, which undergoes shadowed-Rician (SR) fading [61]. n_U denotes the zero mean additive white Gaussian noise (AWGN) with variance ϑ_U^2 at U can be modeled as $n_U \sim \mathcal{CN}\left(0, {\vartheta_U}^2\right)$.

Similarly, the signal received by the satellite from the terrestrial user can be expressed as

$$z_{S_1} = \sqrt{P_U}h_{US}\left(\sqrt{b_1}x_u + \sqrt{b_2}x_{u'}\right) + n_S, \tag{2}$$

where P_U is the transmit power of U, $P_U = \mu P_E$. $h_{US} = h_{SU}$. n_S is the AWGN at S modeled as $n_S \sim \mathcal{CN}\left(0, {\vartheta_S}^2\right)$.

Moreover, the signal received by HAP[7] can be expressed as

$$\begin{aligned} z_H = &\sqrt{P_S}h_{SH}\left(\sqrt{a_1}x_s + \sqrt{a_2}x_{s'}\right) \\ &+ \sqrt{P_U}h_{UH}\left(\sqrt{b_1}x_u + \sqrt{b_2}x_{u'}\right) + n_H \end{aligned}, \tag{3}$$

where h_{SH} is the complex propagation coefficient between the satellite and the HAP. h_{UH} is the complex propagation coefficient between the terrestrial user and the HAP, which can be considered to follow the Nakagami-m fading distribution [27]. n_H is the zero-mean AWGN with variance ϑ_H^2 at HAP.

In the second phase, the HAP decodes the signal received from the satellite and terrestrial user; then, it employs the superposition coding technology to generate the NOMA signal [28]. The superposed signal transmitted by the HAP can be expressed as $y_H = \sqrt{c_1}x_u + \sqrt{c_2}x_s$, which satisfies $E\left[|x_u|^2\right] = E\left[|x_s|^2\right] = 1$. To improve the signal transmission quality, the basic layer signals are superimposed to transmit. c_1 and c_2 are the power allocation coefficients of HAP satisfying $c_1 + c_2 = 1$. Since the link condition between the HAP and the satellite is significantly worse than that between the HAP and the user, more power will be allocated to transmit x_u, i.e., $c_1 > c_2$. Therefore, the signal received by the satellite in the second phase can be expressed as [62]

$$z_{S_2} = \sqrt{P_H}h_{HS}\left(\sqrt{c_1}x_u + \sqrt{c_2}x_s\right) + n_S, \tag{4}$$

where P_H is the transmit power of H, $P_H = \mu P_E$, and $h_{HS} = h_{SH}$.

The signal received by the terrestrial user in the second phase can be denoted as [62]

$$z_{U_2} = \sqrt{P_H}h_{HU}\left(\sqrt{c_1}x_u + \sqrt{c_2}x_s\right) + n_U, \tag{5}$$

where $h_{HU} = h_{UH}$.

B. Imperfect CSI and SIC

In the entire signal propagation process, it is difficult for the system to acquire perfect CSI due to shadow fading, scattering and other reasons [52]. Channel estimation error often occurs in the channel estimation processing, thus so after using the traditional method of estimating the CSI of transmission, the

[4]The terrestrial user is assumed as a small IoT or IoV device, which is equipped with a single antenna [53].

[5]Owing to obstacles, weather conditions like rain, fog and the other reasons, only one direct link is considered in this paper, which is a widely used assumption [24], [25].

[6]By utilizing NOMA, which can transmit a two-layered signal through one resource block. Compared with single-layered signals, the layered coding technology encodes one signal into a two-layered signal, which can improve the spectrum efficiency of the system. In addition, the SIC technology can be adopted in the receiver to decode the layered signal [48].

[7]Since the HAP simultaneously receives signals from two signal sources, the signals will interfere with each other when they are decoded [46].

channel coefficient can be defined as

$$h_{\mathcal{C}} = \tilde{h}_{\mathcal{C}} + e_{\mathcal{C}}, \mathcal{C} \in \{SH, HU, SU\}, \tag{6}$$

where $h_{\mathcal{C}}$ is the realistic channel coefficient between nodes, $\tilde{h}_{\mathcal{C}}$ is the estimated channel coefficient, and $e_{\mathcal{C}}$ shows the degree of imperfect CSI, which obeys $e_{\mathcal{C}} \sim \mathcal{CN}(0, \kappa_e)$. $e_{\mathcal{C}}$ and $\tilde{h}_{\mathcal{C}}$ are mutually orthogonal to each other. Using the pilot symbols to estimate the CSI, with the linear minimum mean-square error (MMSE) algorithm [50], κ_e can be expressed as

$$\kappa_e = E\left[|h_{\mathcal{C}}|^2\right] - E\left[\left|\tilde{h}_{\mathcal{C}}\right|^2\right] = \frac{1}{L\overline{\upsilon}_{\mathcal{C}} + 1}, \tag{7}$$

where L is the length of the pilot symbol. $\overline{\upsilon}_{\mathcal{C}} = E\{\upsilon_{\mathcal{C}}\} = P_{\mathcal{C}} E\left\{|h_{\mathcal{C}}|^2\right\} / \vartheta_{\mathcal{C}}^2$, and $P_{\mathcal{C}} = (1-\mu)P_E$ is the power for channel estimation.

SIC is the conventional method to decode the superposed signal [55]. However, SIC technology must rely on strong receiver performance. The terrestrial user and satellite cannot satisfy this requirement. Thus, we assume that imperfect SIC appears at S and U.

Under these circumstances, the SINR of decoding the superposed signal from U at S can be obtained. Firstly, the basic layer signal with more allocated power is decoded as

$$\gamma_{S_1-u} = \frac{\mu b_1 \gamma_{SU}}{\mu b_2 \gamma_{SU} + \mu\kappa_e + 1}, \tag{8}$$

where $\gamma_{SU} = \bar{\gamma}_{SU}|h_{SU}|^2$, $\bar{\gamma}_{SU} = P_E/\vartheta_S^2$.

Then, the additional layer signal with less allocated power is decoded; due to imperfect SIC at S, the basic layer signal cannot be totally eliminated. Thus, the SINR of $x_{u'}$ is given by

$$\gamma_{S_1-u'} = \frac{\mu b_2 \gamma_{SU}}{\mu\xi b_1 \gamma_{SU} + \mu\kappa_e + 1}, \tag{9}$$

where $\xi \in (0,1)$ shows the imperfect degree of SIC.

Similarly, the SINR of decoding the superposed signal from S at U can be obtained separately by

$$\gamma_{U_1-s} = \frac{\mu a_1 \gamma_{US}}{\mu a_2 \gamma_{US} + \mu\kappa_e + 1}, \tag{10}$$

and

$$\gamma_{U_1-s'} = \frac{\mu a_2 \gamma_{US}}{\mu\xi a_1 \gamma_{US} + \mu\kappa_e + 1}, \tag{11}$$

where $\gamma_{US} = \bar{\gamma}_{US}|h_{US}|^2$, $\bar{\gamma}_{US} = P_E/\vartheta_U^2$.

At the HAP[8], with decoding x_s as an example, the SINR can be expressed as

$$\gamma_{H-s} = \frac{\mu a_1 \gamma_{HS}}{\mu a_2 \gamma_{HS} + \varpi(\mu b_1 \gamma_{HU} + \mu b_2 \gamma_{HU}) + \mu\kappa_e + 1}, \tag{12}$$

where $\varpi \in (0,1)$ describes the interference factor. $\gamma_{HS} = \bar{\gamma}_{HS}|h_{HS}|^2$, $\bar{\gamma}_{HS} = P_E/\vartheta_H^2$. $\gamma_{HU} = \bar{\gamma}_{HU}|h_{HU}|^2$ and $\bar{\gamma}_{HU} = P_E/\vartheta_H^2$.

[8]In this paper, it is assumed that the HAP has strong receiver performance, so imperfect SIC is not considered. However, the decoded signal at the HAP will be interfered by another source signal.

Similarly, we can obtain

$$\gamma_{H-s'} = \frac{\mu a_2 \gamma_{HS}}{\varpi(\mu b_1 \gamma_{HU} + \mu b_2 \gamma_{HU}) + \mu\kappa_e + 1}, \tag{13}$$

$$\gamma_{H-u} = \frac{\mu b_1 \gamma_{HU}}{\mu b_2 \gamma_{HU} + \varpi(\mu a_1 \gamma_{HS} + \mu a_2 \gamma_{HS}) + \mu\kappa_e + 1}, \tag{14}$$

and

$$\gamma_{H-u'} = \frac{\mu b_2 \gamma_{HU}}{\varpi(\mu a_1 \gamma_{HS} + \mu a_2 \gamma_{HS}) + \mu\kappa_e + 1}. \tag{15}$$

In the second phase, the SINR for decoding signal x_u at S can be obtained as

$$\gamma_{S_2-u} = \frac{\mu c_1 \gamma_{SH}}{\mu c_2 \gamma_{SH} + \mu\kappa_e + 1}, \tag{16}$$

where $\gamma_{SH} = \bar{\gamma}_{SH}|h_{SH}|^2$, $\bar{\gamma}_{SH} = P_E/\vartheta_S^2$.

At U, x_u is first decoded; then, x_s is obtained under imperfect SIC, and the SINRs can be expressed as

$$\gamma_{U_2-u} = \frac{\mu c_1 \gamma_{UH}}{\mu c_2 \gamma_{UH} + \mu\kappa_e + 1}, \tag{17}$$

and

$$\gamma_{U_2-s} = \frac{\mu c_2 \gamma_{UH}}{\mu\xi c_1 \gamma_{UH} + \mu\kappa_e + 1}, \tag{18}$$

where $\gamma_{UH} = \bar{\gamma}_{UH}|h_{SH}|^2$, $\bar{\gamma}_{UH} = P_E/\vartheta_U^2$.

C. Statistical Properties of Channels

In this subsection, the statistical properties of channels will be presented.

1) Satellite-HAP/User links: The propagation model of the satellite to the HAP/user links h_S, $S \in \{SU, SH\}$, undergoes SR fading as follows [61]

$$h_S = \sqrt{F_S Q_S}\mathcal{R}_S^{-\frac{1}{2}} \cdot G_S^{\frac{1}{2}} g_S, \tag{19}$$

where $\mathcal{R}_S$ shows the rain attenuation, which modeled as lognormal random distribution, i.e., $\mathcal{R}_S \sim \mathcal{CN}(\varepsilon, \vartheta_{\mathcal{R}}^2)$. $F_S = \left(\frac{\mathcal{V}}{f}\right)^2 \frac{1}{\left(d_S^2 + d_h^2\right)\varsigma_S}$ is a scaling constant with $\mathcal{V}=c/4\pi$, c is the electromagnetic wave velocity, f is the frequency of the signal carrier, d_S is the vertical distance from a GEO satellite to the receiving equipment plane, and d_h is the horizontal distance between the receiving equipment and the center of the satellite antenna coverage area center. $\varsigma_S = KT_p$ denotes the free space path loss (FSPL) factor. $K = 1.380649 \times 10^{-23} J/K$ is Boltzmann constant, T_p is the propagation path's noise temperature, and Q_S is the receive antenna gain, which can be given by

$$Q_S \simeq \begin{cases} G_{R\max} - 2.5 \times 10^{-3}\left(\frac{d_R\theta}{\lambda}\right)^2, & 0^\circ < \theta < \theta_a \\ 2 + 15\log\frac{d_R}{\lambda}, & \theta_a < \theta < \theta_b \\ 32 - 25\log\theta, & \theta_b < \theta < 48^\circ \\ -10, & 48^\circ < \theta < 180^\circ \end{cases}, \tag{20}$$

where $G_{R\max}$ is the maximum receive antenna gain; d_R is the diameter of the receive antenna, θ is the angle of off-boresight

for the receive antenna. $\theta_a = \frac{20\lambda}{d_R}\sqrt{\mathcal{G}_{\max} - \left(2 + 15\log\frac{d_R}{\lambda}\right)}$ and $\theta_b = 15.85\left(\frac{d_R}{\lambda}\right)^{-0.6}$ are two angle values. Next, $G_S = G_{T\max}(\frac{K_1(\rho)}{2\rho} + 36\frac{K_3(\rho)}{\rho^3})^2$ is the transmit antenna gain of satellite; $G_{T\max}$ is the maximum transmit antenna gain of satellite; $K_n, n \in (1,3)$ is the first-kind Bessel function with order n. $\rho = \frac{2.07123\sin\sigma}{\sin\sigma_{3dB}}$, where σ is the angle between the center of the transmit beam and the receive user antenna. Without loss of generality, to obtain the best antenna gain, we adopt the maximum gain in each node.

g_S describes the channel coefficient for SR fading of the satellite to the HAP/user links. SR fading has been proven to be well consistent with the measured satellite signal transmission channel [61]. In addition, SR fading has less calculation complexity than other models. Hence, SR fading model is widely used in [29], [31], [51].

The PDF of $\gamma_S = \bar{\gamma}_S|h_S|^2$ can be given by [61]

$$f_{\gamma_S}(x) = \alpha_S \sum_{k=0}^{m_S-1} \frac{\zeta(k)}{\bar{\gamma}_S^{k+1}} x^k e^{-\Delta_S x}, \tag{21}$$

where $\zeta(k) = (-1)^k(1-m_S)_k\delta_S^k/(k!)^2$, $(\cdot)_k$ is Pochhammer symbol, $\Delta_S = (\beta_S - \delta_S)/\bar{\gamma}_S$. $\alpha_S \triangleq \left(\frac{2b_S m_S}{2b_S m_S + \Omega_S}\right)^{m_S}/2b_S$, $\beta_S \triangleq \frac{1}{2b_S}$, $\delta_S \triangleq \frac{\Omega_S}{2b_S(2b_S m_{SU_p} + \Omega_S)}$, $m_S \in (0,\infty)$ is the fading severity factor. When $m_S \to \infty$, the shadowed-Rician channel will be reduced to the Rician fading. Besides, Ω_S and $2b_S$ are the average powers of the LOS and scatter element, respectively.

Using [63, Eq. 3.351.2], the cumulative distribution function (CDF) of γ_S can be deduced as

$$F_{\gamma_S}(x) = 1 - \alpha_S \sum_{k=0}^{m_S-1} \frac{\zeta(k)}{\bar{\gamma}_S^{k+1}} \sum_{t=0}^{k} \frac{k!}{t!}\Delta_S^{-(k+1-t)} x^t e^{-\Delta_S x}. \tag{22}$$

2) HAP-User links: The propagation model of the HAP-to-user link h_{HU} follows Nakagami-m distribution, which can be defined as [27]

$$h_{HU} = \Theta_{HU} Q_{HU} g_{HU}, \tag{23}$$

where g_{HU} is the channel coefficient for Nakagami-m fading of the HAP-to-user link. Q_{HU} is the channel propagation element during the HAP-to-user link, which can be expressed as

$$Q_{HU} = G_H + G_U + 10\lg(\lambda/4\pi) - 5\varsigma_{HU}\lg\sqrt{d_H^2 + d_u^2}, \tag{24}$$

where G_H and G_U are the transmit antenna gain of the HAP and receive antenna gain of U, respectively. λ is the wavelength of the signal. ς_{HU} is the FSPL of the HAP-to-user link. d_H is the height of the HAP, and d_u is the horizontal distance from the user to the center of the HAP beam. Θ_{HU} shows the three-dimensional positional relationship between the HAP and the terrestrial user. To facilitate the understanding of the distance and angular relationship between the HAP and the terrestrial user, a three-dimensional coordinate system is built with the HAP as the coordinate origin. Then, we can readily mark the coordinates of U as (x_U, y_U, z_U). The angular relationship between the HAP antenna and the user antenna can also be obtained: $\varphi_U \in [0, 2\pi)$ shows the azimuth angular between HAP and U, and $\omega_U \in [0, \pi/2)$ depicts the elevation angular between HAP and U. The angular relationship can also be expressed in the form of coordinates as follows

$$\varphi_U = \begin{cases} \arccos\left(x_U \Big/ \sqrt{x_U^2 + y_U^2}\right), & y_U \geq 0 \\ 2\pi - \arccos\left(x_U \Big/ \sqrt{x_U^2 + y_U^2}\right), & y_U < 0 \end{cases}, \tag{25}$$

and

$$\omega_U = \arctan\left(z_U \Big/ \sqrt{x_U^2 + y_U^2}\right). \tag{26}$$

Based on the three-dimensional coordinate system, Θ_{HU} can be expressed as

$$\Theta_{HU} = \Theta_x(\varphi_U, \omega_U) \otimes \Theta_y(\varphi_U, \omega_U), \tag{27}$$

where $\otimes$ denotes the convolution operation. $\Theta_x(\varphi_U, \omega_U)$ and $\Theta_y(\varphi_U, \omega_U)$ denote the horizontal and vertical array steering vectors, respectively.

According to $\gamma_{HU} = \bar{\gamma}_{HU}|h_{HU}|^2$, the PDF of γ_{HU} is given by [27]

$$f_{\gamma_{HU}}(x) = \frac{\Psi_U^{m_U}}{\Gamma(m_U)} x^{m_U-1} e^{-\Psi_U x}, \tag{28}$$

where $\Psi_U = \frac{m_U}{\Omega_U \bar{\gamma}_{HU}}$. m_U and Ω_U denote the fading severity and average power of the HAP-to-U link, respectively.

After an integral transformation, the CDF of γ_{HU} can be expressed as

$$F_{\gamma_{HU}}(x) = 1 - e^{-\Psi_U x} \sum_{k=0}^{m_U-1} \frac{\Psi_U^k x^k}{k!}. \tag{29}$$

III. System Performance

In this section, closed-form expressions for OP and EC are derived through theoretical results to verify the impact on performance at different system parameter settings. Also, to further demonstrate this phenomenon, asymptotic expressions for OP in the high SNR communication environment are further derived.

A. Outage Probability (OP)

The OP is one of the most important factors in the wireless network to describe the performance of the system. In this paper, we adopt strict OP for the entire system, i.e., the SINR to decode a signal at each node must fall below the outage threshold γ_{th} of the system [4].

The outage of the overall system can be mainly divided into two situations: (i) In the first phase, the node is outage, which consists of the satellite decoding decode user signals, user decoding satellite signals, and HAP decoding satellite and user signals. (ii) In the second phase, the node is outage, which consists of satellite failing to decode HAP signals and user failing to decode HAP signals.

Theorem 1. *The OP of the entire system can be written as* (30) *at the top of the next page, where* $\Upsilon_1 = \frac{(\mu\kappa_e+1)\gamma_{th}}{\mu a_1 - \mu a_2\gamma_{th}}$,

$$
\begin{aligned}
P_{out} = 1 - \alpha_S{}^{9} & \sum_{k=0}^{m_S-1} \frac{\zeta(k)}{\bar{\gamma}_S^{k+1}} \sum_{t=0}^{k} \frac{k!}{t!} \Delta_S^{-(k+1-t)} \Upsilon_1{}^{t} e^{-\Delta_S \Upsilon_1} \sum_{k=0}^{m_S-1} \frac{\zeta(k)}{\bar{\gamma}_S^{k+1}} \sum_{t=0}^{k} \frac{k!}{t!} \Delta_S^{-(k+1-t)} \Upsilon_2{}^{t} e^{-\Delta_S \Upsilon_2} \\
& \times \sum_{k=0}^{m_S-1} \frac{\zeta(k)}{\bar{\gamma}_S^{k+1}} \sum_{t=0}^{k} \frac{k!}{t!} \Delta_S^{-(k+1-t)} \Upsilon_3{}^{t} e^{-\Delta_S \Upsilon_3} \sum_{k=0}^{m_S-1} \frac{\zeta(k)}{\bar{\gamma}_S^{k+1}} \sum_{t=0}^{k} \frac{k!}{t!} \Delta_S^{-(k+1-t)} \Upsilon_4{}^{t} e^{-\Delta_S \Upsilon_4} \\
& \times \sum_{k=0}^{m_S-1} \frac{\zeta(k)}{\bar{\gamma}_S^{k+1}} \sum_{t=0}^{k} \frac{k!}{t!} \Delta_S^{-(k+1-t)} \sum_{l=0}^{t} \binom{t}{l} A_1^{l} B_1^{t-l} e^{-\Delta_S B_1} \frac{{\Psi_U}^{m_U}}{\Gamma(m_U)} (l + m_U - 1)! (\Delta_S A_1 + \Psi_U)^{-(l+m_U)} \\
& \times \sum_{k=0}^{m_S-1} \frac{\zeta(k)}{\bar{\gamma}_S^{k+1}} \sum_{t=0}^{k} \frac{k!}{t!} \Delta_S^{-(k+1-t)} \sum_{l=0}^{t} \binom{t}{l} A_2^{l} B_2^{t-l} e^{-\Delta_S B_2} \frac{{\Psi_U}^{m_U}}{\Gamma(m_U)} (l + m_U - 1)! (\Delta_S A_2 + \Psi_U)^{-(l+m_U)} \\
& \times \sum_{k=0}^{m_S-1} \frac{\zeta(k)}{\bar{\gamma}_S^{k+1}} \left(k! \Delta_S^{-k-1} - e^{-\Psi_U B_3} \sum_{t=0}^{m_U-1} \sum_{l=0}^{t} \frac{{\Psi_U}^{t} A_3^{l} B_3^{t-l} (k+l)!}{t! (\Psi_U A_3 + \Delta_S)^{k+l+1}} \right) \\
& \times \sum_{k=0}^{m_S-1} \frac{\zeta(k)}{\bar{\gamma}_S^{k+1}} \left(k! \Delta_S^{-k-1} - e^{-\Psi_U B_4} \sum_{t=0}^{m_U-1} \sum_{l=0}^{t} \frac{{\Psi_U}^{t} A_4^{l} B_4^{t-l} (k+l)!}{t! (\Psi_U A_4 + \Delta_S)^{k+l+1}} \right) \\
& \times e^{-\Psi_U (\Upsilon_5 + \Upsilon_6)} \sum_{l_1=0}^{m_U-1} \frac{{\Psi_U}^{l_1} {\Upsilon_6}^{l_1}}{l_1!} \sum_{l_2=0}^{m_U-1} \frac{{\Psi_U}^{l_2} {\Upsilon_5}^{l_2}}{l_2!} \sum_{k=0}^{m_S-1} \frac{\zeta(k)}{\bar{\gamma}_S^{k+1}} \sum_{t=0}^{k} \frac{k!}{t!} \Delta_S^{-(k+1-t)} \Upsilon_5{}^{t} e^{-\Delta_S \Upsilon_5}
\end{aligned}
\tag{30}
$$

$\Upsilon_2 = \frac{(\mu\kappa_e+1)\gamma_{th}}{\mu a_2 - \mu\xi a_1 \gamma_{th}}$, $\Upsilon_3 = \frac{(\mu\kappa_e+1)\gamma_{th}}{\mu b_1 - \mu b_2 \gamma_{th}}$, $\Upsilon_4 = \frac{(\mu\kappa_e+1)\gamma_{th}}{\mu b_2 - \mu\xi b_1 \gamma_{th}}$, $\Upsilon_5 = \frac{(\mu\kappa_e+1)\gamma_{th}}{\mu c_1 - \mu c_2 \gamma_{th}}$, $\Upsilon_6 = \frac{(\mu\kappa_e+1)\gamma_{th}}{\mu c_2 - \mu\xi c_1 \gamma_{th}}$, $A_1 = \frac{\varpi\gamma_{th}}{a_1 - a_2\gamma_{th}}$, $B_1 = \frac{(\mu\kappa_e+1)\gamma_{th}}{\mu a_1 - \mu a_2 \gamma_{th}}$, $A_2 = \frac{\varpi\gamma_{th}}{a_2}$, $B_2 = \frac{(\mu\kappa_e+1)\gamma_{th}}{\mu a_2}$, $A_3 = \frac{\varpi\gamma_{th}}{b_1 - b_2\gamma_{th}}$, $B_3 = \frac{(\mu\kappa_e+1)\gamma_{th}}{\mu b_1 - \mu b_2 \gamma_{th}}$, $A_4 = \frac{\varpi\gamma_{th}}{b_2}$, *and* $B_4 = \frac{(\mu\kappa_e+1)\gamma_{th}}{\mu b_2}$.

Proof: The proof is relegated into Appendix A. ■

B. Asymptotic OP

To gain more insight of the OP, the asymptotic analysis for the OP in high SNR regime is investigated.

Based on the CDF expressions for SR fading and Nakagami-m fading, when the average SNR of the channel approaches infinity, the CDF expressions in high SNR regime are respectively, rewritten as

$$F_{\gamma_S}^{\infty}(x) \overset{\Delta}{\simeq} \frac{\alpha_S}{\bar{\gamma}_S} x, \tag{31}$$

and

$$F_{\gamma_{HU}}^{\infty}(x) \overset{\Delta}{\simeq} \frac{\Psi_U^{m_U}}{\Gamma(m_U)} x^{m_U}. \tag{32}$$

Lemma 1. *The asymptotic OP of the entire system is given as (33), which is seen at the top of the next page.*

Proof: See Appendix B. ■

C. Ergodic Capacity

The EC is another expression of link capacity. When the link capacity cannot meet the required user rate, an interruption event is generated, which is probabilistically distributed, depending on the average signal-to-noise ratio of the link and its channel fading distribution model, and is one of the important evaluation indicators of the system performance. [31]. In this paper, there are two transmission links: the user-to-satellite link and the satellite-to-user link. The EC of the user-to-satellite link can be defined as

$$EC_S = EC_{SU} + \min\{EC_{HU}, EC_{SH}\}, \tag{34}$$

where EC_{SU} denotes the EC of the direct link. EC_{HU} and EC_{SH} are two links in the two-way HAP-forward link, which help spread the signal of the user to the satellite.

Proof: The proof is relegated into Appendix C. ■

Finally, by substituting (36), (37) and (38) into (34), we obtain the EC of the user-to-satellite link.

Similarly, the EC of the satellite-to-user link is

$$EC_U = EC_{US} + \min[EC_{HS}, EC_{UH}], \tag{35}$$

where EC_{US} is the EC of the direct link from the satellite to the user. EC_{HS} and EC_{UH} are the ECs of two links in the two-way HAP-forward link, which help spread the signal of the satellite to the user. Using similar derivations in Appendix C, we obtain the final EC of the satellite-to-user link.

Theorem 2. *The final expression of EC_{SU}, EC_{HU} and EC_{SH} are derived as (36), (37) and (38), respectively. (36) and (37) are shown at top of next page.*

$$
\begin{aligned}
EC_{SH} = & \frac{\alpha_S}{2\ln 2} \sum_{k=0}^{m_S-1} \frac{\zeta(k)}{\bar{\gamma}_S^{k+1} \Delta_S^{k+1}} \\
& \left[G_{23}^{31}\left(\frac{\mu\kappa_e+1}{\mu} \Delta_S \middle| \begin{matrix} 0, 1 \\ 1+k, 0, 0 \end{matrix} \right) - G_{23}^{31}\left(\frac{\mu\kappa_e+1}{\mu c_2} \Delta_S \middle| \begin{matrix} 0, 1 \\ 1+k, 0, 0 \end{matrix} \right) \right]
\end{aligned}
\tag{38}
$$

IV. Numerical & Simulation Results

In this section, some representative Monte Carlo simulations are provided to validate the outage behavior and EC of the two-way satellite-HAP-terrestrial network. In addition, the influences of key parameters, i.e., the power allocation coefficient, channel conditions, imperfect CSI, imperfect SIC, and interference factor, on the system performance are revealed. Without loss of generality, we set $a_1 = b_1 = c_1$, $a_2 = b_2 = c_2$, $\overline{\gamma}_{SU} = \overline{\gamma}_{SH} = \overline{\gamma}_{HU} = \overline{\gamma}$, $\vartheta_{SU}^2 = \vartheta_{SH}^2 = \vartheta_{HU}^2 = 1$, $m_{SU} = m_{SH} = m_S$, $b_{SU} = b_{SH} = b_S$, $\Omega_{SU} = \Omega_{SH} = \Omega_S$, and $\Omega_U = 1$ [23], [29]. In addition, the detailed system and channel parameters are shown in Table I and Table II, respectively [27], [37], [59].

Fig. 2 illustrates the OP of the system versus a_1 for different SR shadow fading conditions under $\xi = 0.01$, $L = 5$, $\mu = 0.75$, $\gamma_{th} = 1$dB, $\varpi = 0.01$ and $m_U = 1$. Firstly, the numerical simulation results are observed to be in agreement with the theoretical analysis, which verifies the correctness of

$$P_{out}^{asy} = 1 - \frac{\alpha_S^9}{\bar{\gamma}_S^9}\Upsilon_1\Upsilon_2\Upsilon_3\Upsilon_4\Upsilon_5^{m_U+1}\Upsilon_6^{m_U}\left(A_1\bar{\gamma}_S + B_1\right)\left(A_2\bar{\gamma}_S + B_2\right)\left(\frac{{\Psi_U}^{m_U}}{\Gamma(m_U+1)}\right)^2 \sum_{t_1=0}^{m_U}\binom{m_U}{t_1} A_3^{t_1} B_3^{m_U-t_1} \times \sum_{k_1=0}^{m_S-1}\frac{\zeta(k_1)}{\bar{\gamma}^{k_1+1}}(k_1+t)!{\Delta_S}^{-(k_1+t)-1}\sum_{t_2=0}^{m_U}\binom{m_U}{t_2} A_3^{t_2} B_3^{m_U-t_2}\sum_{k_2=0}^{m_S-1}\frac{\zeta(k_2)}{\bar{\gamma}^{k_2+1}}(k_2+t)!{\Delta_S}^{-(k_2+t)-1}\left(\frac{{\Psi_U}^{m_U}}{\Gamma(m_U)}\right)^2. \quad (33)$$

$$EC_{SU} = \frac{\alpha_S}{\ln 2}\sum_{k=0}^{m_S-1}\frac{\zeta(k)}{\bar{\gamma}_S^{k+1}{\Delta_S}^{k+1}}\left[G_{23}^{31}\left(\frac{\mu\kappa_e+1}{\mu}\Delta_S\middle|\begin{matrix}0,1\\1+k,0,0\end{matrix}\right) - G_{23}^{31}\left(\frac{\mu\kappa_e+1}{\mu b_2}\Delta_S\middle|\begin{matrix}0,1\\1+k,0,0\end{matrix}\right) + G_{23}^{31}\left(\frac{\mu\kappa_e+1}{\mu(b_2+\xi b_1)}\Delta_S\middle|\begin{matrix}0,1\\1+k,0,0\end{matrix}\right) - G_{23}^{31}\left(\frac{\mu\kappa_e+1}{\mu\xi b_1}\Delta_S\middle|\begin{matrix}0,1\\1+k,0,0\end{matrix}\right)\right]. \quad (36)$$

$$EC_{HU} = \frac{\alpha_S}{2\ln 2}\sum_{k=0}^{m_S-1}\frac{\zeta(k)}{\bar{\gamma}_S^{k+1}}\left[\sum_{t=0}^{m_U-1}\binom{m_U-1}{t}\left(\frac{\Delta_S}{C_2}-\frac{\Psi_U}{C_1}\right)^{-(k+t+1)}(-1)^t(k+t)! \times \frac{{\Psi_U}^t{C_1}^{-t}{C_2}^{-k-1}}{\Gamma(m_U)}G_{23}^{31}\left(\frac{\Psi_U}{C_1}\middle|\begin{matrix}0,1\\m_U-t,0,0\end{matrix}\right) - \frac{1}{\Delta_S^{k+1}}G_{23}^{31}\left(\frac{\mu\kappa_e+1}{\varpi\mu}\Delta_S\middle|\begin{matrix}0,1\\1+k,0,0\end{matrix}\right)\right]. \quad (37)$$

TABLE I
SYSTEM PARAMETERS

Satellite height	d_S=35786km
HAP height	d_H=20km
Frequency	f=2GHz
Bandwidth	B=15MHz
Noise temperature	T=300K
Satellite transmit gain	$G_{T\max}$=48dB
Receive gain	$G_{R\max}$=4dB
3dB angle	$\theta_{3\text{dB}}$=0.5°

TABLE II
SR FADING CHANNEL PARAMETERS

Shadowing	m_S	b_S	Ω_S
Frequent heavy shadowing (FHS)	1	0.063	0.0007
Average shadowing (AS)	5	0.251	0.279
Infrequent light shadowing (ILS)	10	0.158	1.29

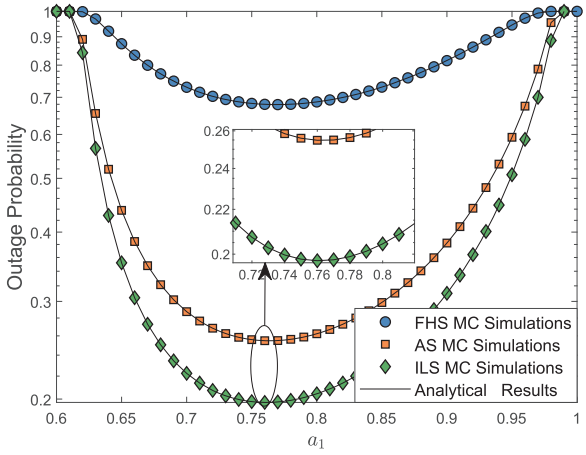

Fig. 2. OP of the system versus $\overline{\gamma}$ for different power allocation coefficients.

our theoretical derivations. Then, when the satellite channel suffers light shadowing, the OP decreases. In addition, the OP of the system achieves the better performance at $a_1 = 0.76$. Thus, the optimal power allocation coefficients is set as $a_1 = 0.76$ and $a_2 = 0.24$ in the following simulations.

Fig. 3 depicts the OP of the system versus $\overline{\gamma}$ for different SR shadow fading and Nakagami-m shadow fading under $a_1 = 0.76$, $a_2 = 0.24$, $\xi = 0.01$, $L = 5$, $\mu = 0.75$, $\gamma_{th} = 1$dB and $\varpi = 0.01$. The asymptotic results are identical to the simulation results in a high-SNR regime, which validates the exactness of our asymptotic derivations. Similar to Fig. 2, the outage performance improves when the SR fading improves. The OP of the system decreases when m_U increases under the AS and ILS scenarios. However, the outage performance of $m_U = 1$ is better than that of $m_U = 2$ in the FHS scenario. This result can be explained that in the FHS scenario: with the m_U increasing, the interference impact on the satellite-HAP link increases, so the system is more easily interrupted. When the SR channel suffers AS or ILS shadowing, the increase in m_U has a relatively small impact on the interference of the satellite-HAP link.

Fig. 4 plots the OP of the system versus ξ for different $\overline{\gamma}$ and Nakagami-m shadow fading conditions under $a_1 = 0.76$, $a_2 = 0.24$, $L = 5$, $\mu = 0.75$, $\gamma_{th} = 1$dB, $\varpi = 0.01$ and the FHS scenario. According to $\gamma_{th} < \frac{a_2}{\xi a_1}$, the value of ξ must be less than 0.25. We observe that the performance for the OP of the system will deteriorate when ξ increases. Regardless of how the channel condition or SNR is improved, when $\xi > 0.22$, the OP of the system will be close to 1. This result enlightens that performing perfect SIC can effectively enhance the performance of the OP for the considered system.

Fig. 5 illustrates the OP of the system versus ϖ for different L and SR shadow fading conditions under $a_1 = 0.76$, $a_2 = 0.24$, $\xi = 0.01$, $\mu = 0.75$, $\gamma_{th} = 1$dB and $m_U = 1$. The observed interference factor ϖ significantly impacts the OP performance of the system. When $\varpi > 0.1$, the system cannot complete normal communication. Moreover, from the enlarged simulation results, the performance of the OP for the considered system is enhanced with L increasing.

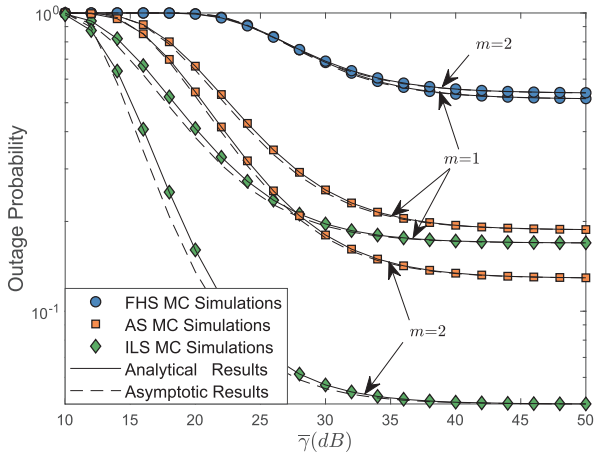

Fig. 3. OP versus $\overline{\gamma}$ for different SR shadow fading and Nakagami-m shadow fading conditions.

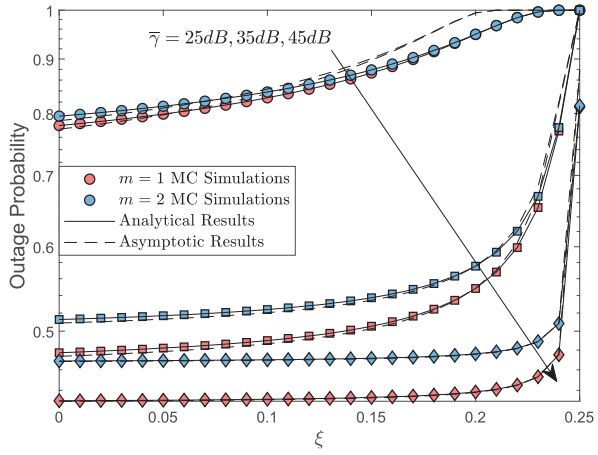

Fig. 4. OP versus ξ for different Nakagami-m shadow fading conditions.

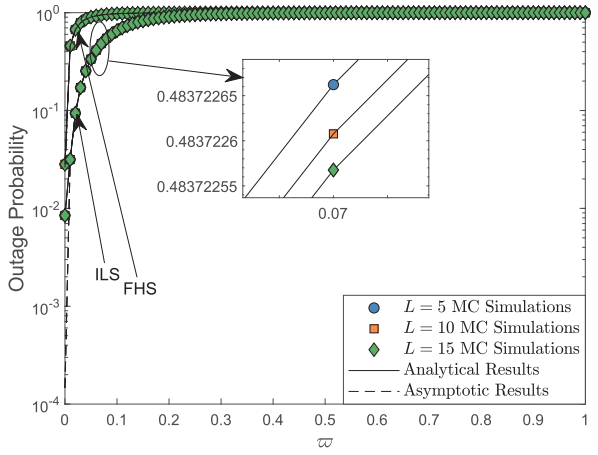

Fig. 5. OP versus ϖ for different lengths of pilot symbol L and SR shadow fading.

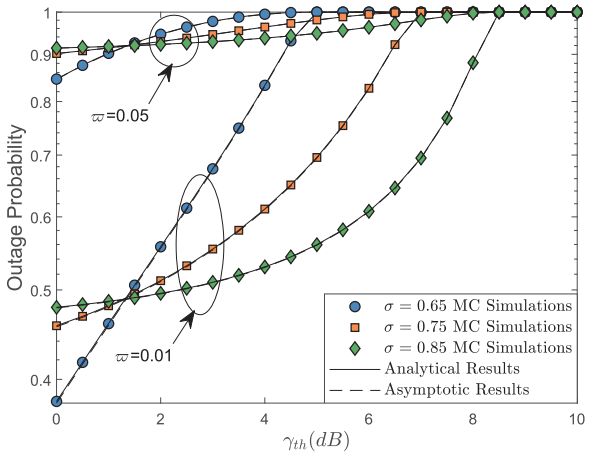

Fig. 6. OP versus γ_{th} for different signal power coefficients μ and interference factors ϖ.

Fig. 6 shows the OP of the system versus γ_{th} for different μ and ϖ values under $a_1 = 0.76$, $a_2 = 0.24$, $\xi = 0.01$, $L = 5$, $m_U = 1$ and the FHS scenario. A higher system outage threshold corresponds to higher requirements for the outage performance of the system. In addition, the outage threshold affects the power allocation factor. When $\gamma_{th} < 1.5$ dB, the performance for the OP of the considered system enhances with μ decreasing. However, when $\gamma_{th} > 1.5$ dB, the performance for the OP of the considered system enhances with μ increasing. The reason is that the system will allocate more power to transmit signals when the system has higher requirements for outage performance.

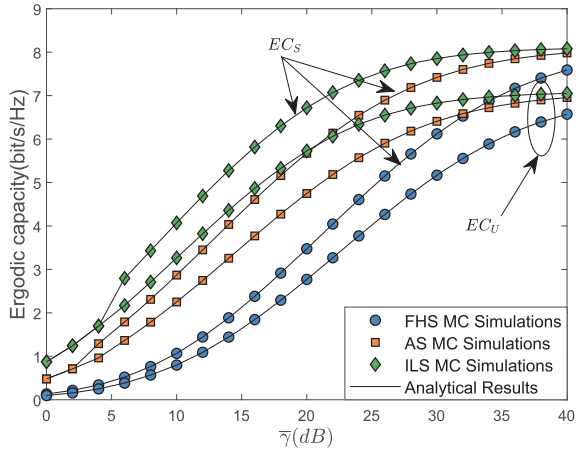

Fig. 7. EC of S and U versus $\overline{\gamma}$ for different SR shadow fading conditions.

Fig. 7 elaborates the ECs of the satellite and user versus $\overline{\gamma}$ for different SR shadow fading conditions under $a_1 = 0.76$, $a_2 = 0.24$, $\xi = 0.01$, $L = 5$, $\mu = 0.75$, $\varpi = 0.01$ and $m_U = 1$. The simulation results are consistent with the analytical results, which prove the accuracy of our analytical derivations of EC. Moreover, the ECs of the satellite and user elevate that when the SR suffers light fading, and the EC from the user to the satellite is larger than that of link between the satellite

and the user, since the two-way HAP allocates more power to transmit the user signal in a superposed signal under the NOMA scheme.

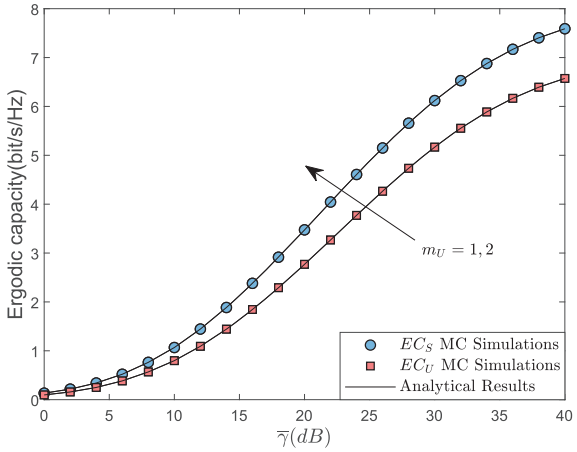

Fig. 8. EC of S and U versus $\overline{\gamma}$ for different Nakagami-m shadow fading conditions.

Fig. 8 depicts the ECs of the satellite and user versus $\overline{\gamma}$ for different Nakagami-m shadow fading conditions under $a_1 = 0.76$, $a_2 = 0.24$, $\xi = 0.01$, $L = 5$, $\mu = 0.75$, $\varpi = 0.01$ and the FHS scenario. We observe that, the Nakagami-m shadow fading has no effect on the EC of the satellite and user. The reason is that the EC is mainly affected by the direct link, and the two-way HAP link is restricted by the minimum value of the two links. Therefore, only improving the channel condition between HAP and user cannot improve the EC of the entire link.

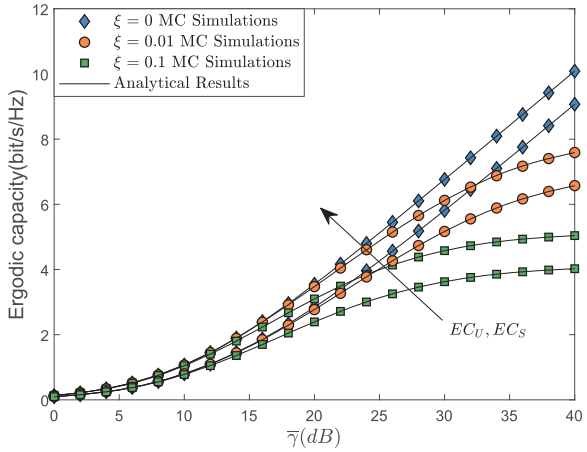

Fig. 9. EC of S and U versus $\overline{\gamma}$ for different SIC imperfections.

Fig. 9 examines the ECs of the satellite and user versus $\overline{\gamma}$ for different SIC imperfections under $a_1 = 0.76$, $a_2 = 0.24$, $L = 5$, $\mu = 0.75$, $\varpi = 0.01$, $m_U = 1$ and the FHS scenario. As expected, the EC performance strongly deteriorates with the increase in imperfect SIC coefficient. At 40 dB, the EC under $\xi = 0.1$ is only half of that with perfect SIC.

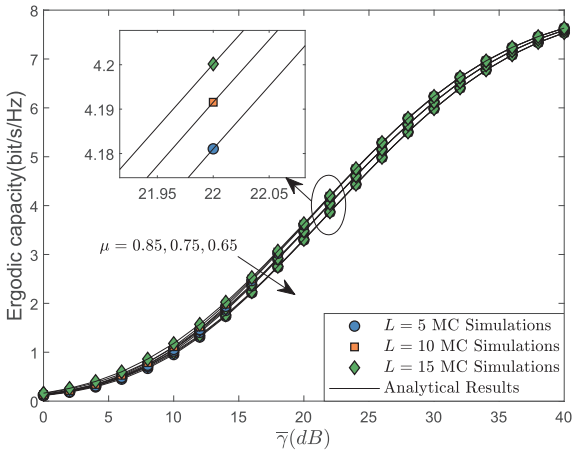

Fig. 10. EC of S and U versus $\overline{\gamma}$ for different CSI imperfections.

Fig. 10 depicts the ECs of the satellite and user versus $\overline{\gamma}$ for different CSI imperfections under $a_1 = 0.76$, $a_2 = 0.24$, $\xi = 0.01$, $\varpi = 0.01$, $m_U = 1$ and the FHS scenario. When the system allocates more power to signal transmission, the ECs of the satellite and user increase. In addition, with the increasing the length of the pilot symbol, the EC is enhanced.

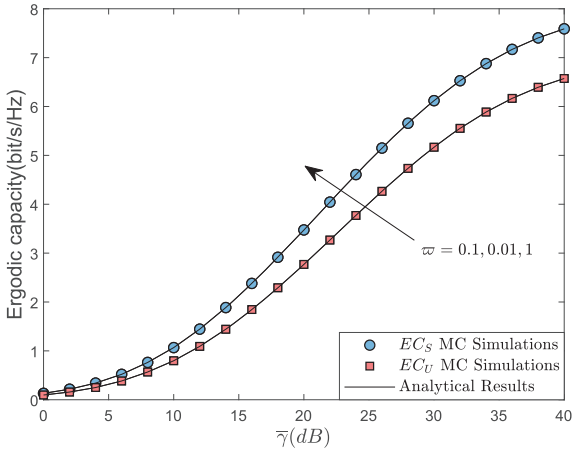

Fig. 11. EC of S and U versus $\overline{\gamma}$ for different interference factors.

Fig. 11 plots the ECs of the satellite and user versus $\overline{\gamma}$ for different ϖ values under $a_1 = 0.76$, $a_2 = 0.24$, $\xi = 0.01$, $L = 5$, $\mu = 0.75$, $m_U = 1$ and the FHS scenario. Similar to Fig. 8, the effect of interference on the two-way HAP link does not greatly influence the ECs of the satellite and user.

V. Conclusions

In this paper, we investigated the performance of a two-way satellite-HAP-terrestrial network with NOMA and imperfect limitations. Closed-form expressions for the OP and EC of the considered system were theoretically derived to quantify the system performance. In addition, asymptotic expressions for the OP in high-SNR regimes were obtained to gain deeper insight. MC results were performed to evaluate the correctness

of our theoretical analysis and the impacts of key parameters on the system. The simulations determined the optimal power allocation coefficient of the NOMA scheme. The imperfect CSI and SIC strongly affected the system deterioration, which could not be ignored in reality.

ACKNOWLEDGMENTS

We thank LetPub (www.letpub.com) for linguistic assistance and pre-submission expert review.

APPENDIX A
PROOF OF THEOREM 1

The OP of the entire system is defined as

$$P_{out} = P_{out}^{1} + P_{out}^{2} - P_{out}^{1}P_{out}^{2}, \tag{39}$$

where $P_{out}^{1} = P_S + P_U - P_S P_U$ is the OP of the first phase, and P_S and P_U are the OPs of the nodes that receive the satellite signal and terrestrial user signal.

Then, P_S can be expressed as

$$P_S = P_{U-S} + P_{H-S} - P_{U-S}P_{H-S}, \tag{40}$$

where P_{U-S} and P_{H-S} show the OPs of the terrestrial user and HAP for decoding the superposed signal from the satellite. P_{U-S} can be defined as

$$P_{U-S} = P_{U-s} + P_{U-s'} - P_{U-s}P_{U-s'}, \tag{41}$$

where $P_{U-s} = \Pr\{\gamma_{U_1-s} < \gamma_{th}\}$ and $P_{U-s'} = \Pr\{\gamma_{U_1-s'} < \gamma_{th}\}$.

Using (10), the expression of P_{U-s} can be derived as

$$\begin{aligned} P_{U-s} &= \Pr\left\{\gamma_{U_1-s} < \gamma_{th}\right\} \\ &= \Pr\left\{\gamma_{US} < \tfrac{(\mu\kappa_e+1)\gamma_{th}}{\mu a_1 - \mu a_2\gamma_{th}}\right\} = F_{\gamma_{US}}\left(\Upsilon_1\right) \end{aligned}, \tag{42}$$

where $\Upsilon_1 = \frac{(\mu\kappa_e+1)\gamma_{th}}{\mu a_1 - \mu a_2\gamma_{th}}$, $\gamma_{th} < \frac{a_1}{a_2}$. If $\gamma_{th} > \frac{a_1}{a_2}$, the node will always experience outage.

Recalling the CDF expression in (22), the expression can be rewritten as

$$P_{U-s} = \alpha_S \sum_{k=0}^{m_S-1} \frac{\zeta\left(k\right)}{\bar{\gamma}_S^{k+1}} \sum_{t=0}^{k} \frac{k!}{t!} \Delta_S^{-(k+1-t)} {\Upsilon_1}^t e^{-\Delta_S \Upsilon_1}. \tag{43}$$

Similarly, the other OPs can be obtained as

$$\begin{aligned} P_{U-s'} &= \Pr\left\{\gamma_{U_1-s'} < \gamma_{th}\right\} \\ &= \Pr\left\{\gamma_{US} < \tfrac{(\mu\kappa_e+1)\gamma_{th}}{\mu a_2 - \mu\xi a_1\gamma_{th}}\right\} = F_{\gamma_{US}}\left(\Upsilon_2\right) \\ &= \alpha_S \sum_{k=0}^{m_S-1} \tfrac{\zeta(k)}{\bar{\gamma}_S^{k+1}} \sum_{t=0}^{k} \tfrac{k!}{t!} \Delta_S^{-(k+1-t)} {\Upsilon_2}^t e^{-\Delta_S \Upsilon_2} \end{aligned}, \tag{44}$$

where $\Upsilon_2 = \frac{(\mu\kappa_e+1)\gamma_{th}}{\mu a_2 - \mu\xi a_1\gamma_{th}}$, $\gamma_{th} < \frac{a_2}{\xi a_1}$.

$$\begin{aligned} P_{S-u} &= \Pr\left\{\gamma_{S_1-u} < \gamma_{th}\right\} \\ &= \Pr\left\{\gamma_{SU} < \tfrac{(\mu\kappa_e+1)\gamma_{th}}{\mu b_1 - \mu b_2\gamma_{th}}\right\} = F_{\gamma_{SU}}\left(\Upsilon_3\right) \\ &= \alpha_S \sum_{k=0}^{m_S-1} \tfrac{\zeta(k)}{\bar{\gamma}_S^{k+1}} \sum_{t=0}^{k} \tfrac{k!}{t!} \Delta_S^{-(k+1-t)} {\Upsilon_3}^t e^{-\Delta_S \Upsilon_3} \end{aligned}, \tag{45}$$

where $\Upsilon_3 = \frac{(\mu\kappa_e+1)\gamma_{th}}{\mu b_1 - \mu b_2\gamma_{th}}$, $\gamma_{th} < \frac{b_1}{b_2}$.

$$\begin{aligned} P_{S-u'} &= \Pr\left\{\gamma_{S_1-u'} < \gamma_{th}\right\} \\ &= \Pr\left\{\gamma_{SU} < \tfrac{(\mu\kappa_e+1)\gamma_{th}}{\mu b_2 - \mu\xi b_1\gamma_{th}}\right\} = F_{\gamma_{SU}}\left(\Upsilon_4\right) \\ &= \alpha_S \sum_{k=0}^{m_S-1} \tfrac{\zeta(k)}{\bar{\gamma}_S^{k+1}} \sum_{t=0}^{k} \tfrac{k!}{t!} \Delta_S^{-(k+1-t)} {\Upsilon_4}^t e^{-\Delta_S \Upsilon_4} \end{aligned}, \tag{46}$$

where $\Upsilon_4 = \frac{(\mu\kappa_e+1)\gamma_{th}}{\mu b_2 - \mu\xi b_1\gamma_{th}}$, $\gamma_{th} < \frac{b_2}{\xi b_1}$.

$$\begin{aligned} P_{S_2-u} &= \Pr\left\{\gamma_{S_2-u} < \gamma_{th}\right\} \\ &= \Pr\left\{\gamma_{SH} < \tfrac{(\mu\kappa_e+1)\gamma_{th}}{\mu c_1 - \mu c_2\gamma_{th}}\right\} = F_{\gamma_{SH}}\left(\Upsilon_5\right) \\ &= \alpha_S \sum_{k=0}^{m_S-1} \tfrac{\zeta(k)}{\bar{\gamma}_S^{k+1}} \sum_{t=0}^{k} \tfrac{k!}{t!} \Delta_S^{-(k+1-t)} {\Upsilon_5}^t e^{-\Delta_S \Upsilon_5} \end{aligned}, \tag{47}$$

where $\Upsilon_5 = \frac{(\mu\kappa_e+1)\gamma_{th}}{\mu c_1 - \mu c_2\gamma_{th}}$, satisfying $\gamma_{th} < \frac{c_1}{c_2}$.

Unlike the above derivations, the HAP is accompanied by interference when decoding signals. Therefore, P_{H-s} can be expressed as

$$\begin{aligned} P_{H-s} &= \Pr\left\{\gamma_{H-s} < \gamma_{th}\right\} \\ &= \Pr\left\{\gamma_{SH} < \tfrac{\varpi\mu\gamma_{th}\gamma_{HU} + (\mu\kappa_e+1)\gamma_{th}}{\mu a_1 - \mu a_2\gamma_{th}}\right\} \\ &= F_{\gamma_{SH}}\left(A_1\gamma_{HU} + B_1\right) \\ &= \int_0^{\infty} F_{\gamma_{SH}}\left(A_1 y + B_1\right) f_{\gamma_{HU}}\left(y\right) dy \end{aligned}, \tag{48}$$

where $A_1 = \frac{\varpi\gamma_{th}}{a_1 - a_2\gamma_{th}}$, and $B_1 = \frac{(\mu\kappa_e+1)\gamma_{th}}{\mu a_1 - \mu a_2\gamma_{th}}$.

By resorting to the CDF of SR fading and PDF of Nakagami-m fading, using [63, Eq. 1.111 and Eq. 3.351.3], we can recast P_{H-s} to

$$\begin{aligned} P_{H-s} = \alpha_S \sum_{k=0}^{m_S-1} \tfrac{\zeta(k)}{\bar{\gamma}_S^{k+1}} \sum_{t=0}^{k} \tfrac{k!}{t!} \Delta_S^{-(k+1-t)} \sum_{l=0}^{t} \binom{t}{l} A_1^l B_1^{t-l} \\ \times e^{-\Delta_S B_1} \tfrac{{\Psi_U}^{m_U}}{\Gamma(m_U)} (l+m_U-1)! (\Delta_S A_1 + \Psi_U)^{-(l+m_U)} \end{aligned}. \tag{49}$$

By utilizing similar derivations, we obtain $P_{H-s'}$ as

$$\begin{aligned} P_{H-s'} = \alpha_S \sum_{k=0}^{m_S-1} \tfrac{\zeta(k)}{\bar{\gamma}_S^{k+1}} \sum_{t=0}^{k} \tfrac{k!}{t!} \Delta_S^{-(k+1-t)} \sum_{l=0}^{t} \binom{t}{l} A_2^l B_2^{t-l} \\ \times e^{-\Delta_S B_2} \tfrac{{\Psi_U}^{m_U}}{\Gamma(m_U)} (l+m_U-1)! (\Delta_S A_2 + \Psi_U)^{-(l+m_U)} \end{aligned}, \tag{50}$$

where $A_2 = \frac{\varpi\gamma_{th}}{a_2}$, and $B_2 = \frac{(\mu\kappa_e+1)\gamma_{th}}{\mu a_2}$.

Similarly, P_{H-u} and $P_{H-u'}$ can be, respectively, derived as

$$\begin{aligned} P_{H-u} = \alpha_S \sum_{k=0}^{m_S-1} \tfrac{\zeta(k)}{\bar{\gamma}_S^{k+1}} \\ \times \left(k! \Delta_S^{-k-1} - e^{-\Psi_U B_3} \sum_{t=0}^{m_U-1} \sum_{l=0}^{t} \tfrac{{\Psi_U}^t A_3^l B_3^{t-l} (k+l)!}{t! (\Psi_U A_3 + \Delta_S)^{k+l+1}} \right) \end{aligned}, \tag{51}$$

where $A_3 = \frac{\varpi\gamma_{th}}{b_1 - b_2\gamma_{th}}$ and $B_3 = \frac{(\mu\kappa_e+1)\gamma_{th}}{\mu b_1 - \mu b_2\gamma_{th}}$.

$$\begin{aligned} P_{H-u'} = \alpha_S \sum_{k=0}^{m_S-1} \tfrac{\zeta(k)}{\bar{\gamma}_S^{k+1}} \\ \times \left(k! \Delta_S^{-k-1} - e^{-\Psi_U B_4} \sum_{t=0}^{m_U-1} \sum_{l=0}^{t} \tfrac{{\Psi_U}^t A_4^l B_4^{t-l} (k+l)!}{t! (\Psi_U A_4 + \Delta_S)^{k+l+1}} \right) \end{aligned}, \tag{52}$$

where $A_4 = \frac{\varpi\gamma_{th}}{b_2}$ and $B_4 = \frac{(\mu\kappa_e+1)\gamma_{th}}{\mu b_2}$.

In the HAP-to-user link, the channel undergoes Nakagami-

m fading. By resorting to the CDF of Nakagami-m fading, the expressions of P_{U_2-u} and P_{U_2-s} can be, respectively, as

$$\begin{aligned} P_{U_2-u} &= \Pr\{\gamma_{U_2-u} < \gamma_{th}\} \\ &= \Pr\left\{\gamma_{HU} < \frac{(\mu\kappa_e+1)\gamma_{th}}{\mu c_1 - \mu c_2\gamma_{th}}\right\} = F_{\gamma_{HU}}(\Upsilon_5) \\ &= e^{-\Psi_U\Upsilon_5}\sum_{k=0}^{m_U-1}\frac{{\Psi_U}^k{\Upsilon_5}^k}{k!} \end{aligned}, \quad (53)$$

$$\begin{aligned} P_{U_2-s} &= \Pr\{\gamma_{U_2-s} < \gamma_{th}\} \\ &= \Pr\left\{\gamma_{HU} < \frac{(\mu\kappa_e+1)\gamma_{th}}{\mu c_2 - \mu\xi c_1\gamma_{th}}\right\} = F_{\gamma_{HU}}(\Upsilon_6) \\ &= e^{-\Psi_U\Upsilon_6}\sum_{k=0}^{m_U-1}\frac{{\Psi_U}^k{\Upsilon_6}^k}{k!} \end{aligned}, \quad (54)$$

where $\Upsilon_6 = \frac{(\mu\kappa_e+1)\gamma_{th}}{\mu c_2 - \mu\xi c_1\gamma_{th}}$, $\gamma_{th} < \frac{c_2}{\xi c_1}$.

Based on (43) and (44), we obtain the OP for the terrestrial users as

$$P_{U-S} = P_{U-s} + P_{U-s'} - P_{U-s}P_{U-s'}. \quad (55)$$

By using (49) and (50), we obtain the OP for the HAP by decoding the satellite signal as

$$P_{H-S} = P_{H-s} + P_{H-s'} - P_{H-s}P_{H-s'}. \quad (56)$$

Therefore, the OP of the nodes that receive the satellite signal can be obtained as (57), which is shown at the top of the next page.

Similarly, from (45) and (46), we derive the OP for the satellite by decoding the legitimate users' signal as

$$P_{S-U} = P_{S-u} + P_{S-u'} - P_{S-u}P_{S-u'}. \quad (58)$$

From (51) and (52), the OP for the HAP by decoding the satellite signal can be obtained as

$$P_{H-U} = P_{H-u} + P_{H-u'} - P_{H-u}P_{H-u'}. \quad (59)$$

Thus, the OP of the nodes that receive the user signal can be given by (60) at the top of the next page.

Owing to the utilization of DF protocol, the OP of the first phase is obtained as

$$P_{out}^1 = P_S + P_U - P_S P_U. \quad (61)$$

Recalling (53) and (54), the OP for the user by decoding the HAP signal in the second phase can be denoted by

$$P_{U_2} = P_{U_2-u} + P_{U_2-s} - P_{U_2-u}P_{U_2-s}. \quad (62)$$

Using (47), the OP of the second phase is derived as

$$P_{out}^2 = P_{U_2} + P_{S_2-u} - P_{U_2}P_{S_2-u}. \quad (63)$$

The detailed expression of P_{out}^2 is given by (64), which can be seen at the top of the next page.

Finally, by substituting the OP expressions of each phase into (39), the final expression of the entire system is given as (30).

The proof is completed.

Appendix B
Proof of Lemma 1

Firstly, we replace (22) and (29) with (31) and (32), respectively. Then, by using the similar method of Appendix A, the asymptotic OP of the node under SR fading can be written as

$$P_{U-s}^{\infty} = \frac{\alpha_S}{\bar{\gamma}_S}\Upsilon_1, \quad (65)$$

$$P_{U-s'}^{\infty} = \frac{\alpha_S}{\bar{\gamma}_S}\Upsilon_2, \quad (66)$$

$$P_{S-u}^{\infty} = \frac{\alpha_S}{\bar{\gamma}_S}\Upsilon_3, \quad (67)$$

$$P_{S-u'}^{\infty} = \frac{\alpha_S}{\bar{\gamma}_S}\Upsilon_4, \quad (68)$$

and

$$P_{S_2-u}^{\infty} = \frac{\alpha_S}{\bar{\gamma}_S}\Upsilon_5. \quad (69)$$

Hence, the asymptotic OP of the HAP node under interference can be, respectively, given as

$$P_{H-s}^{\infty} = \alpha_S A_1 + \frac{\alpha_S}{\bar{\gamma}}B_1, \quad (70)$$

$$P_{H-s'}^{\infty} = \alpha_S A_2 + \frac{\alpha_S}{\bar{\gamma}}B_2, \quad (71)$$

$$\begin{aligned} P_{H-u}^{\infty} = &\frac{{\Psi_U}^{m_U}}{\Gamma(m_U+1)}\sum_{t=0}^{m_U}\binom{m_U}{t}A_3^t B_3^{m_U-t} \\ &\times\alpha_S\sum_{k=0}^{m_S-1}\frac{\zeta(k)}{\bar{\gamma}^{k+1}}(k+t)!{\Delta_S}^{-(k+t)-1} \end{aligned}, \quad (72)$$

and

$$\begin{aligned} P_{H-u'}^{\infty} = &\frac{{\Psi_U}^{m_U}}{\Gamma(m_U+1)}\sum_{t=0}^{m_U}\binom{m_U}{t}A_4^t B_4^{m_U-t} \\ &\times\alpha_S\sum_{k=0}^{m_S-1}\frac{\zeta(k)}{\bar{\gamma}^{k+1}}(k+t)!{\Delta_S}^{-(k+t)-1} \end{aligned}. \quad (73)$$

In addition, the asymptotic OP of the node under Nakagami-m fading can be, respectively, derived as

$$P_{U_2-u}^{\infty} = \frac{{\Psi_U}^{m_U}}{\Gamma(m_U)}\Upsilon_5^{m_U}, \quad (74)$$

$$P_{U_2-s}^{\infty} = \frac{{\Psi_U}^{m_U}}{\Gamma(m_U)}\Upsilon_6^{m_U}. \quad (75)$$

Finally, recalling the closed-form expression for the OP in each phase, we obtain the asymptotic expression for the OP of the entire system.

The proof is completed.

Appendix C
Proof of Theorem 2

EC_{SU} is defined as

$$EC_{SU} = E\left[\log_2(1+\gamma_{S_1-u})\right] + E\left[\log_2(1+\gamma_{S_1-u'})\right]. \quad (76)$$

By substituting the SINR of γ_{S_1-u} and $\gamma_{S_1-u'}$ into (76) and using the logarithmic function operation rules, we obtain

$$\begin{aligned} EC_{SU} = &\frac{1}{\ln 2}\left\{E\left[\ln\left(\frac{\mu\gamma_{US}}{\mu\kappa_e+1}+1\right)\right] - E\left[\ln\left(\frac{\mu b_2\gamma_{US}}{\mu\kappa_e+1}+1\right)\right]\right. \\ &\left.+E\left[\ln\left(\frac{\mu(b_2+\xi b_1)\gamma_{US}}{\mu\kappa_e+1}+1\right)\right] - E\left[\ln\left(\frac{\mu\xi b_1\gamma_{US}}{\mu\kappa_e+1}+1\right)\right]\right\} \end{aligned}. \quad (77)$$

For brevity, we define $E\left[\ln\left(\frac{\mu\gamma_{US}}{\mu\kappa_e+1}+1\right)\right] = I_1$, $\gamma_{US} = x_1$, and $\frac{\mu\gamma_{US}}{\mu\kappa_e+1} = z_1$. After an integral operation, the PDF of

$$P_S = 1 - {\alpha_S}^4 \sum_{k=0}^{m_S-1} \frac{\zeta(k)}{\bar{\gamma}_S^{k+1}} \sum_{t=0}^{k} \frac{k!}{t!} \Delta_S^{-(k+1-t)} {\Upsilon_1}^t e^{-\Delta_S \Upsilon_1} \sum_{k=0}^{m_S-1} \frac{\zeta(k)}{\bar{\gamma}_S^{k+1}} \sum_{t=0}^{k} \frac{k!}{t!} \Delta_S^{-(k+1-t)} {\Upsilon_2}^t e^{-\Delta_S \Upsilon_2}$$
$$\times \sum_{k=0}^{m_S-1} \frac{\zeta(k)}{\bar{\gamma}_S^{k+1}} \sum_{t=0}^{k} \frac{k!}{t!} \Delta_S^{-(k+1-t)} \sum_{l=0}^{t} \binom{t}{l} A_1^l B_1^{t-l} e^{-\Delta_S B_1} \frac{{\Psi_U}^{m_U}}{\Gamma(m_U)} (l+m_U-1)! (\Delta_S A_1 + \Psi_U)^{-(l+m_U)} \quad , \tag{57}$$
$$\times \sum_{k=0}^{m_S-1} \frac{\zeta(k)}{\bar{\gamma}_S^{k+1}} \sum_{t=0}^{k} \frac{k!}{t!} \Delta_S^{-(k+1-t)} \sum_{l=0}^{t} \binom{t}{l} A_2^l B_2^{t-l} e^{-\Delta_S B_2} \frac{{\Psi_U}^{m_U}}{\Gamma(m_U)} (l+m_U-1)! (\Delta_S A_2 + \Psi_U)^{-(l+m_U)}$$

$$\begin{aligned} P_U &= P_{S-U} + P_{H-U} - P_{S-U} P_{H-U} \\ &= 1 - {\alpha_S}^4 \sum_{k=0}^{m_S-1} \frac{\zeta(k)}{\bar{\gamma}_S^{k+1}} \sum_{t=0}^{k} \frac{k!}{t!} \Delta_S^{-(k+1-t)} {\Upsilon_3}^t e^{-\Delta_S \Upsilon_3} \sum_{k=0}^{m_S-1} \frac{\zeta(k)}{\bar{\gamma}_S^{k+1}} \sum_{t=0}^{k} \frac{k!}{t!} \Delta_S^{-(k+1-t)} {\Upsilon_4}^t e^{-\Delta_S \Upsilon_4} \\ &\times \sum_{k=0}^{m_S-1} \frac{\zeta(k)}{\bar{\gamma}_S^{k+1}} \left(k! \Delta_S^{-k-1} - e^{-\Psi_U B_3} \sum_{t=0}^{m_U-1} \sum_{l=0}^{t} \frac{{\Psi_U}^t A_3^l B_3^{t-l} (k+l)!}{t! (\Psi_U A_3 + \Delta_S)^{k+l+1}} \right) \\ &\times \sum_{k=0}^{m_S-1} \frac{\zeta(k)}{\bar{\gamma}_S^{k+1}} \left(k! \Delta_S^{-k-1} - e^{-\Psi_U B_4} \sum_{t=0}^{m_U-1} \sum_{l=0}^{t} \frac{{\Psi_U}^t A_4^l B_4^{t-l} (k+l)!}{t! (\Psi_U A_4 + \Delta_S)^{k+l+1}} \right) \end{aligned} \quad . \tag{60}$$

$$P_{out}^2 = 1 - \alpha_S e^{-\Psi_U(\Upsilon_5+\Upsilon_6)} \sum_{l_1=0}^{m_U-1} \frac{{\Psi_U}^{l_1} {\Upsilon_6}^{l_1}}{l_1!} \sum_{l_2=0}^{m_U-1} \frac{{\Psi_U}^{l_2} {\Upsilon_5}^{l_2}}{l_2!} \sum_{k=0}^{m_S-1} \frac{\zeta(k)}{\bar{\gamma}_S^{k+1}} \sum_{t=0}^{k} \frac{k!}{t!} \Delta_S^{-(k+1-t)} {\Upsilon_5}^t e^{-\Delta_S \Upsilon_5}. \tag{64}$$

z_1 can be obtained as

$$f_{z_1}(z) = \frac{\mu\kappa_e + 1}{\mu} f_{\gamma_{US}} \left(\frac{\mu\kappa_e + 1}{\mu} z \right). \tag{78}$$

By substituting the PDF expression of $f_{\gamma_{US}}$ into (78), we can rewrite $f_{z_1}(z)$ as

$$f_{z_1}(z) = \alpha_S \sum_{k=0}^{m_S-1} \frac{\zeta(k)}{\bar{\gamma}_S^{k+1}} \left(\frac{\mu\kappa_e + 1}{\mu} \right)^{k+1} z^k e^{-\Delta_S \frac{\mu\kappa_e+1}{\mu} z}. \tag{79}$$

In addition, I_1 can be expressed in an integral form as

$$I_1 = \int_0^\infty \ln(z+1) f_{z_1}(z) dz. \tag{80}$$

Using the Meijer's G function defined in [63, Eq. 9.301] and [64, Eq. 8.4.6.5], we obtain

$$\ln(1+z) = G_{22}^{12} \left(z \middle| \begin{matrix} 1, & 1 \\ 1, & 0 \end{matrix} \right). \tag{81}$$

By substituting (79) and (81) into (80) and using [64, Eq. 2.24.3.1], after some mathematical steps, we can obtain I_1 as

$$I_1 = \alpha_S \sum_{k=0}^{m_S-1} \frac{\zeta(k)}{\bar{\gamma}_S^{k+1} \Delta_S^{k+1}} G_{23}^{31} \left(\frac{\mu}{(\mu\kappa_e + 1)\Delta_S} \middle| \begin{matrix} -k, 1, 1 \\ 1, 0 \end{matrix} \right). \tag{82}$$

To avoid the case where the equation cannot hold when $\bar{\gamma}_{SU} = 0$, we utilize [64, Eq. 8.2.2.14] to rewrite the expression, which is shown as

$$I_1 = \alpha_S \sum_{k=0}^{m_S-1} \frac{\zeta(k)}{\bar{\gamma}_S^{k+1} \Delta_S^{k+1}} G_{23}^{31} \left(\frac{\mu\kappa_e + 1}{\mu} \Delta_S \middle| \begin{matrix} 0, 1 \\ 1+k, 0, 0 \end{matrix} \right). \tag{83}$$

With the similar method, we obtain the remaining components

$$\begin{aligned} I_2 &= E\left[\ln\left(\tfrac{\mu b_2 \gamma_{US}}{\mu\kappa_e + 1} + 1 \right) \right] \\ &= \alpha_S \sum_{k=0}^{m_S-1} \frac{\zeta(k)}{\bar{\gamma}_S^{k+1} \Delta_S^{k+1}} G_{23}^{31} \left(\tfrac{\mu\kappa_e+1}{\mu b_2} \Delta_S \middle| \begin{matrix} 0, 1 \\ 1+k, 0, 0 \end{matrix} \right), \end{aligned} \tag{84}$$

$$\begin{aligned} I_3 &= E\left[\ln\left(\tfrac{\mu(b_2 + \xi b_1)\gamma_{US}}{\mu\kappa_e + 1} + 1 \right) \right] \\ &= \alpha_S \sum_{k=0}^{m_S-1} \frac{\zeta(k)}{\bar{\gamma}_S^{k+1} \Delta_S^{k+1}} G_{23}^{31} \left(\tfrac{\mu\kappa_e+1}{\mu(b_2+\xi b_1)} \Delta_S \middle| \begin{matrix} 0, 1 \\ 1+k, 0, 0 \end{matrix} \right), \end{aligned} \tag{85}$$

and

$$\begin{aligned} I_4 &= E\left[\ln\left(\tfrac{\mu\xi b_1 \gamma_{US}}{\mu\kappa_e + 1} + 1 \right) \right] \\ &= \alpha_S \sum_{k=0}^{m_S-1} \frac{\zeta(k)}{\bar{\gamma}_S^{k+1} \Delta_S^{k+1}} G_{23}^{31} \left(\tfrac{\mu\kappa_e+1}{\mu\xi b_1} \Delta_S \middle| \begin{matrix} 0, 1 \\ 1+k, 0, 0 \end{matrix} \right). \end{aligned} \tag{86}$$

Therefore, by inserting (83), (84), (85) and (86) into (77), we obtain the final expression of EC_{SU}.

Since the HAP adopts the half duplex DF protocol, EC_{HU} can be re-written as

$$EC_{HU} = \frac{1}{2} \left\{ E\left[\log_2(1 + \gamma_{H-u}) \right] + E\left[\log_2(1 + \gamma_{H-u'}) \right] \right\}. \tag{87}$$

By inserting (14) and (15) into Eq. (87), after some logarithmic function operations, we can re-write EC_{HU} as

$$EC_{HU} = \frac{1}{2\ln 2} \times \left\{ E\left[\ln\left(\tfrac{\mu\gamma_{UH}}{\mu\kappa_e+1} + \tfrac{\varpi\mu\gamma_{SH}}{\mu\kappa_e+1} + 1 \right) \right] - E\left[\ln\left(\tfrac{\varpi\mu\gamma_{SH}}{\mu\kappa_e+1} + 1 \right) \right] \right\}. \tag{88}$$

For further analysis, we define $C_1 = \frac{\mu}{\mu\kappa_e+1}$, $C_2 = \frac{\varpi\mu}{\mu\kappa_e+1}$, $\gamma_{UH} = x_2$, $\gamma_{SH} = x_3$, and $y_1 = C_1 x_2 + C_2 x_3$. Recalling the

PDF expressions of SR fading and Nakagami-m fading, after some integral steps, we derive the PDF of $f_{y_1}(y)$ as

$$\begin{aligned} f_{y_1}(y) &= \int_0^\infty \frac{1}{C_1 C_2} f_{x_2}\left(\frac{y-v}{C_1}\right) f_{x_3}\left(\frac{v}{C_2}\right) dv \\ &= \alpha_S \sum_{k=0}^{m_S-1} \frac{\zeta(k)}{\bar{\gamma}_S^{k+1}} \frac{{\Psi_U}^{m_U}}{\Gamma(m_U)} \sum_{t=0}^{m_U-1} \binom{m_U-1}{t} (-1)^t (k+t)! \cdot \\ &\times \left(\frac{\Delta_S}{C_2} - \frac{\Psi_U}{C_1}\right)^{-(k+t+1)} {C_1}^{-m_U} {C_2}^{-k-1} y^{m_U-t-1} e^{-\frac{\Psi_U}{C_1} y} \end{aligned} \tag{89}$$

Using Meijer-G function again, we obtain

$$\begin{aligned} I_5 &= E\left[\ln\left(\frac{\mu\gamma_{UH}}{\mu\kappa_e+1} + \frac{\varpi\mu\gamma_{SH}}{\mu\kappa_e+1} + 1\right)\right] \\ &= \int_0^\infty \ln(y+1) f_{y_1}(y) dy \\ &= \alpha_S \sum_{k=0}^{m_S-1} \frac{\zeta(k)}{\bar{\gamma}_S^{k+1}} \sum_{t=0}^{m_U-1} \binom{m_U-1}{t} \left(\frac{\Delta_S}{C_2} - \frac{\Psi_U}{C_1}\right)^{-(k+t+1)} \cdot \\ &\times (-1)^t (k+t)! \frac{{\Psi_U}^t {C_1}^{-t} {C_2}^{-k-1}}{\Gamma(m_U)} G_{23}^{31}\left(\frac{\Psi_U}{C_1} \middle| \begin{matrix} 0, 1 \\ m_U - t, 0, 0 \end{matrix}\right) \end{aligned} \tag{90}$$

Similarly, we obtain

$$\begin{aligned} I_6 &= E\left[\ln\left(\frac{\varpi\mu\gamma_{SH}}{\mu\kappa_e+1} + 1\right)\right] \\ &= \alpha_S \sum_{k=0}^{m_S-1} \frac{\zeta(k)}{\bar{\gamma}_S^{k+1} \Delta_S^{k+1}} G_{23}^{31}\left(\frac{\mu\kappa_e+1}{\varpi\mu}\Delta_S \middle| \begin{matrix} 0, 1 \\ 1+k, 0, 0 \end{matrix}\right) \end{aligned} \tag{91}$$

By substituting (90) and (91) into (88), we obtain the final expression of EC_{HU}.

Similar to deducing EC_{SU} and EC_{HU}, the expression of EC_{SH} can be obtained.

The proof is completed.

REFERENCES

[1] D. Tse and P. Viswanath, *Fundamentals of Wireless Communication*, Cambridge, U.K.: Cambridge Univ. Press, 2005.

[2] B. Li, Z. Fei, C. Zhou, and Y. Zhang, "Physical-layer security in space information networks: A survey," *IEEE Internet Things J.*, vol. 7, no. 1, pp. 33-52, Jan. 2020.

[3] K. Guo et al., "Performance analysis of hybrid satellite-terrestrial cooperative networks with relay selection," *IEEE Trans. Veh. Technol.*, vol. 69, no. 8, pp. 9053-9067, Aug. 2020.

[4] G. Pan, J. Ye, Y. Zhang, M.-S. Alouini, "Performance analysis and optimization of cooperative satellite-aerial-terrestrial systems," *IEEE Trans. Wireless Commun.*, vol. 19, no. 10, pp. 6693-6707, Oct. 2020.

[5] K. Guo, X. Li, M. Alazab, R. H. Jhaveri and K. An, "Integrated satellite multiple two-way relay networks: Secrecy performance under multiple eves and vehicles with non-ideal hardware," *IEEE Trans. Intelligent Vehi.*, vol. 8, no. 2, pp. 1307-1318, Feb. 2023.

[6] K. Guo, C. Dong, and K. An, "NOMA-based cognitive satellite terrestrial relay network: Secrecy performance under channel estimation errors and hardware impairments," *IEEE Internet Things J.*, vol. 9, no. 18, pp. 17334-17347, Sep. 2022.

[7] Y. Ruan, Y. Zhang, Y. Li, R. Zhang, and R. Hang, "An adaptive channel division MAC protocol for high dynamic UAV networks," *IEEE Sens. J.*, vol. 20, no. 16, pp. 9528-9539, Aug. 2020.

[8] B. Li, Z. Fei, and Y. Zhang, "UAV communications for 5G and beyond: Recent advances and future trends," *IEEE Internet Things J.*, vol. 6, no. 2, pp. 2241-2263, Apr. 2019.

[9] P. K. Sharma and D. Gupta, "Outage performance of multi-UAV relaying-based imperfect hardware hybrid satellite-terrestrial networks," *IEEE Syst. J.*, vol. 16, no. 2, pp. 2311-2314, Jun. 2022.

[10] Q. Huang, M. Lin, J.,-B, Wang, T. A. Tsiftsis, and J. Wang, "Energy efficient beamforming schemes for satellite-aerial-terrestrial networks," *IEEE Trans. Commun.*, vol. 68, no. 6, pp. 3863-3875, Jun. 2020.

[11] Z. Jia, M. Sheng, J. Li, D. Zhou, and Z. Han, "Joint HAP access and LEO satellite backhaul in 6G: Matching game-based approaches," *IEEE J. Sel. Areas Comm.*, vol. 39, no. 4, pp. 1147-1159, Apr. 2021.

[12] X. Yue, Y. Liu, Y. Yao, X. Li, and R. Liu, "Secure communications in a unified non-orthogonal multiple access framework," *IEEE Trans. Wireless Commun.*, vol. 19, no. 3, pp. 2163-2178, Mar. 2020.

[13] L. Yang and M. O. Hasna, "Performance analysis of amplify-and-forward hybrid satellite-terrestrial networks with cochannel interference," *IEEE Trans. Commun.*, vol. 63, no. 12, pp. 5052-5061, Dec. 2015.

[14] Y. Liu, W. Yi, Z. Ding, X. Liu, and D. A . Dobre, "Developing NOMA to next generation multiple access (NGMA): Future vision and research opportunities," *IEEE Wireless Commun.*, vol. 29, no. 6, pp. 120-127, Dec. 2022.

[15] K. Guo, R. Liu, M. Alazab, R. H. Jhaveri, X. Li and M. Zhu, "STAR-RIS-empowered cognitive non-terrestrial vehicle network with NOMA," *IEEE Trans. Intelligent Vehi.*, early access, pp. 1-15, Apr. 2023.

[16] W. Wu, X. Wang, F. Zhou, K.-K. Wong, C. Li, and B. Wang, "Resource allocation for enhancing offloading security in NOMA-enabled MEC networks," *IEEE Syst. J.*, vol. 15, no. 3, pp. 3789-3792, Sep. 2021.

[17] N. Zhao, Y. Li, S. Zhang, Y. Chen, W. Lu, J. Wang, and X. Wang, "Security enhancement for NOMA-UAV networks," *IEEE Trans. Veh. Technol.*, vol. 69, no. 4, pp. 3994-4005, Apr. 2020.

[18] K. Guo, M. Wu, X. Li, "Deep reinforcement learning and NOMA-based multi-objective RIS-assisted IS-UAV-TNs: Trajectory optimization and beamforming design," *IEEE Trans. Intell. Transp. Syst.*, early access, pp. 1-14, May 2023.

[19] X. Li *et al.*, "Physical-layer authentication for ambient backscatter-aided NOMA symbiotic systems," *IEEE Trans. Commun.*, vol. 71, no. 4, pp. 2288-2303, Apr. 2023.

[20] V. Singh and P. K. Upadhyay, "Exploiting cache-free/cache-aided TWR-NOMA in cognitive hybrid satellite-terrestrial networks," *IEEE Trans. Veh. Technol.*, vol. 71, no. 2, pp. 1778-1793, Feb. 2022.

[21] X. Li, Y. Zheng, M. Zeng *et al.*, "Enhancing secrecy performance for STAR-RIS NOMA networks," *IEEE Trans. Veh. Technol.*, vol. 72, no. 2, pp. 2684-2688, Feb. 2023.

[22] Q. Wang et al., "UAV-enabled non-orthogonal multiple access networks for ground-air-ground communications," *IEEE Trans. Green Commun. Netw.*, vol. 6, no. 3, pp. 1340-1354, Sept. 2022.

[23] Z. Lin, M. Lin, J.-B. Wang, T. de. Cola, and J. Wang, "Joint beamforming and power allocation for satellite-terrestrial integrated networks with non-orthogonal multiple access," *IEEE J. Sel. Topics Sig. Processing.*, vol. 13, no. 3, pp. 657-670, Jun. 2019.

[24] K. Guo, K. An, F. Zhou, T. A. Tsiftsis, G. Zheng, and S. Chatzinotas, "On the secrecy performance of NOMA-based integrated satellite multiple-terrestrial relay networks with hardware impairments," *IEEE Trans. Veh. Technol.*, vol. 70, no. 4, pp. 3661-3676, Apr. 2021.

[25] F. Zhou, X. Li, M. Alazab, R. H. Jhaveri and K. Guo, "Secrecy performance for RIS-based integrated satellite vehicle networks with a UAV relay and MRC eavesdropping," *IEEE Trans. Intelligent Vehi.*, vol. 8, no. 2, pp. 1676-1685, Feb. 2023.

[26] H. Zhang, G. Pan, S. Ke, S. Wang, and J. An, "Outage analysis of cooperative satellite-aerial-terrestrial networks with spatially random terminals," *IEEE Trans. Commun.*, vol. 70, no. 7, pp. 4972-4987, Jul. 2022.

[27] Q. Huang, M. Lin, W.-P. Zhu, J. Cheng, and M.-S. Alouini, "Uplink massive access in mixed RF/FSO satellite-aerial-terrestrial networks," *IEEE Trans. Commun.*, vol. 69, no. 4, pp. 2413-2426, Apr. 2021.

[28] N. Zhao, X. Pang, Z. Li, Y. Chen, F. Li, Z. Ding, and M.-S. Alouini, "Joint trajectory and precoding optimization for UAV-assisted NOMA networks," *IEEE Trans. Commun.*, vol. 67, no. 5, pp. 3723-3735, May 2019.

[29] K. Guo, M. Lin, B. Zhang, W.-P. Zhu, J.-B. Wang, and T. A. Tsiftsis, "On the performance of LMS communication with hardware impairments and interference," *IEEE Trans. Commun.*, vol. 67, no. 2, pp. 1490-1505, Feb. 2019.

[30] R. Liu et al., "Resource allocation for NOMA-enabled cognitive satellite-UAV-terrestrial networks with imperfect CSI," *IEEE Trans. Cognit. Commun. Networking*, doi: 10.1109/TCCN.2023.3261311.

[31] Y. Tian, G. Pan, M. A. Kishk, and M.-S. Alouini, "Stochastic analysis of cooperative satellite-UAV communications," *IEEE Trans. Wireless Commun.*, vol. 21, no. 6, pp. 3570-3586, Jun. 2022.

[32] P. K. Sharma, D. Gupta, and D. I. Kim, "Outage performance of 3D mobile UAV caching for hybrid satellite-terrestrial networks," *IEEE Trans. Veh. Technol.*, vol. 70, no. 8, pp. 8280-8285, Aug. 2021.

[33] G. Pan, Y. Jia, J. An, and S. Alouini, "Latency versus reliability in LEO mega-constellations: Terrestrial, aerial, or space Relay," *IEEE Trans. Mobile Comput.*, early access, doi: 10.1109/TMC.2022.3168081.

[34] Z. Lin, M. Lin, T. de. Cola, J.-B. Wang, W.-P. Zhu, and J. Cheng, "Supporting IoT with rate-splitting multiple access in satellite and aerial-

integrated networks," *IEEE Internet Things J.*, vol. 8, no. 14, pp. 11123-11134, Jul. 2021.

[35] W. Wu, F. Zhou, R. Q. Hu, and B. Wang, "Energy-efficient resource allocation for secure NOMA-enabled mobile edge computing networks," *IEEE Trans. Commun.*, vol. 68, no. 1, pp. 493-505, Jan. 2020.

[36] P. Li, "Average secrecy capacity of the reconfigurable intelligent surface-assisted integrated satellite unmanned aerial vehicle relay networks," *Comput. Model Eng. Sci.*, accepted for publication.

[37] X. Li, Q. Wang, H. Peng, H. Zhang, D.-T. Do, K. M. Rabie, R. Kharel, and C. C. Cavalcante, "A unified framework for HS-UAV NOMA networks: Performance analysis and location optimization," *IEEE Access*, vol. 8, pp. 13329-13340, Jan. 2020.

[38] X. Yue and Y. Liu, "Performance analysis of intelligent reflecting surface assisted NOMA networks," *IEEE Trans. Wireless Commun.*, vol. 21, no. 4, pp. 2623-2636, Apr. 2022.

[39] Q. Wang, X. Li, S. Bhatia, Y. Liu, L. T. Alex, *et al.*, "UAV-enabled non-orthogonal multiple access networks for ground-air-ground communications," *IEEE Trans. Green Commun. Netw.*, vol. 6, no. 3, pp. 1340-1354, Sep. 2022.

[40] L. Lv, J. Chen, and Q. Ni, "Cooperative non-orthogonal multiple access in cognitive radio," *IEEE Comm. Lett.*, vol. 20, no. 10, pp. 2059-2062, Oct. 2016.

[41] X. Yan, H. Xiao, K. An, G. Zheng, and W. Tao, "Hybrid satellite terrestrial relay networks with cooperative non-orthogonal multiple access," *IEEE Commun. Lett.*, vol. 22, no. 5, pp. 978-981, May 2018.

[42] C. Xia, Z. Xiang, J. Meng, H. Liu, and G. Pan, "NOMA-assisted cognitive short packet communication with node mobility and imperfect channel estimation," *IEEE Trans. Vehi. Technol.*, early access, pp. 1-11, Apr. 2023.

[43] Z. Yang, P. Yue, S. Wang, G. Pan, and J. An, "Energy-efficient optimization for RIS-asided MIMO covert communications," *IEEE I. Things Joural*, ealy access, pp. 1-1, Apr. 2023.

[44] P. Xu, J. Quan, G. Chen, Z. Yang, Y. Li, and I. Krikidis, "A novel link selection in coordinated direct and buffer-aided relay transmission," *IEEE Trans. Wireless Commun.*, vol. 22, no. 5, pp. 3296-3309, May 2023.

[45] Z. Yang, et al., "A novel hybrid successive interference cancellation for uplink wireless power transfer NOMA in internet of things," *IEEE Trans. Vehi. Technol.*, vol. 72, no. 5, pp. 6090-6102, May 2023.

[46] K. Guo, B. Zhang, Y. Huang, and D. Guo, "Performance analysis of two-way satellite terrestrial relay networks with hardware impairments," *IEEE Wireless Commun. Lett.*, vol. 6, no. 4, pp. 430-433, Aug. 2017.

[47] X. Yue, Y. Liu, S. Kang, A. Nallanathan, and Y. Chen, "Modeling and analysis of two-way relay non-orthogonal multiple access systems," *IEEE Trans. Commun.*, vol. 66, no. 9, pp. 3784-3796, Sep. 2018.

[48] X. Wang, M. Jia, I. W. -H. Ho, Q. Guo, and F. C. M. Lau, "Exploiting full-duplex two-way relay cooperative non-orthogonal multiple access," *IEEE Trans. Commun.*, vol. 67, no. 4, pp. 2716-2729, Apr. 2019.

[49] L. Lv, Q. Wu, Z. Li, N. A.-Dhahir, and J. Chen, "Secure two-way communications via intelligent reflecting surfaces," *IEEE Commun. Lett.*, vol. 25, no. 3, pp. 744-748, Mar. 2021.

[50] X. Li, Q. Wang, M. Liu, J. Li, H. Peng, M. J. Piran, and L. Li, "Cooperative wireless-powered NOMA relaying for B5G IoT networks with hardware impairments and channel estimation errors," *IEEE Internet Things J.*, vol. 8, no. 7, pp. 5453-5467, Apr. 2021.

[51] X. Li, M. Zhao, M. Zeng, S. Mumtaz, V. G. Menon, Z. Ding, and O. A. Dobre, "Hardware impaired ambient backscatter NOMA systems: Reliability and security," *IEEE Trans. Commun.*, vol. 69, no. 4, pp. 2723-2736, Apr. 2021.

[52] Y. Ruan, L. Jiang, Y. Li, and R. Zhang, "Energy-efficient power control for cognitive satellite-terrestrial networks with outdated CSI," *IEEE Syst. J.*, vol. 15, no. 1, pp. 1329-1332, Mar. 2021.

[53] X. Yan, H. Xiao, K. An, G. Zheng, and S. Chatzinotas, "Ergodic capacity of NOMA-based uplink satellite networks with randomly deployed users," *IEEE Syst. J.*, vol. 14, no. 3, pp. 3343-3350, Sep. 2020.

[54] Y. Sun, K. An, J. Luo, Y. Zhu, *et al.*, "Outage constrained robust beamforming optimization for multiuser IRS-assisted anti-jamming communications with incomplete information," *IEEE Internet Things J.*, vol. 9, no. 15, pp. 13298-13314, Aug. 2022.

[55] Z. Ding, R. Schober and H. V. Poor, "Unveiling the importance of SIC in NOMA systems–Part 1: State of the art and recent findings," *IEEE Commun. Lett.*, vol. 24, no. 11, pp. 2373-2377, Nov. 2020.

[56] X. Yue, Z. Qin, Y. Liu, S. Kang, and Y. Chen, "A unified framework for non-orthogonal multiple access," *IEEE Trans. Commun.*, vol. 66, no. 11, pp. 5346-5359, Nov. 2018.

[57] N. S. Mouni, A. Kumar, and P. K. Upadhyay, "Adaptive user pairing for NOMA systems with imperfect SIC," *IEEE Wireless Commun. Lett.*, vol. 10, no. 7, pp. 1547-1551, Jul. 2021.

[58] W. U. Khan, X. Li, M. Zeng, and O. A. Dobre, "Backscatter-enabled NOMA for future 6G systems: A new optimization framework under imperfect SIC," *IEEE Commun. Lett.*, vol. 25, no. 5, pp. 1669-1672, May 2021.

[59] X. Yue, Y. Liu, Y. Yao, T. Li, X. Li, R. Liu, and A. Nallanathan, "Outage behaviors of NOMA-based satellite network over shadowed-rician fading channels," *IEEE Trans. Veh. Technol.*, vol. 69, no. 6, pp. 6818-6821, Jun. 2020.

[60] B. K. S. Lima, D. B. da Costa, L. Yang, F. R. M. Lima, R. Oliveira, and U. S. Dias, "Adaptive power factor allocation for cooperative full-duplex NOMA systems with imperfect SIC and rate fairness," *IEEE Trans. Veh. Technol.*, vol. 69, no. 11, pp. 14061-14066, Nov. 2020.

[61] A. Abdi, W. C. Lau, M. -. Alouini, and M. Kaveh, "A new simple model for land mobile satellite channels: First- and second-order statistics," *IEEE Trans. Wireless Commun.*, vol. 2, no. 3, pp. 519-528, May 2003.

[62] L. Lv, et al., "Multi-antenna two-way relay based cooperative NOMA," *IEEE Trans. Wireless Commun.*, vol. 19, no. 10, pp. 6486-6503, Oct. 2020.

[63] I. S. Gradshteyn, I. M. Ryzhik, A. Jeffrey, and D. Zwillinger, *Table of integrals, series and products*. 7th ed. Amsterdam, Boston: Elsevier, 2007.

[64] A. P. Prudnikov, Y. A. Brychkov, O. I. Marichev, *Integralsand Series, Volume 3: More Special functions*. New York: ser. Gordon and Breach, 1990.

Response to Reviewers' Comments on ID-VT-2023-01441:

Two-Way Satellite-HAP-Terrestrial Networks with Non-Orthogonal Multiple Access

June 28, 2023